Nonlocal Operator Method for Solving Partial Differential Equations: State-of-the-Art Review and Future Perspectives

Yongzheng ZHANG[1], *Huilong REN*[1], *Timon RABCZUK*[1,*]

[1]Institute of Structural Mechanics, Bauhaus-University Weimar, 99423 Weimar, Germany

*Corresponding Author: Timon RABCZUK (Email: timon.rabczuk@uni-weimar.de)
(Received: 4-Dec-2021; accepted: 23-Feb-2022; published: 31-Mar-2022)
DOI:http://dx.doi.org/10.55579/jaec.202261.357

Abstract. *The nonlocal operator method (NOM) is based on nonlocal theory and employs nonlocal operators of integral form to replace the local partial differential operators. NOM naturally bridges models of different length scales and enables also the natural solution of problems with continuous to discontinuous solutions as they occur in the case of material failure. It also provides a natural framework for complex multifield problems. It is based on a variational principle or weighted residual method and only requires the definition of associated energy potential. As the NOM does not require any shape functions as 'traditional methods' such as FEM, IGA or meshfree methods, its implementation is significantly simplified. It has been successfully applied to the solution of several partial differential equations (PDEs). This paper aims to provide a comprehensive description of the NOM together with a review of its major applications for the solution of PDEs for challenging engineering problems. Finally, we give some potential future research direction in the area of methods based on nonlocal operators.*

Keywords

Nonlocal operator method, nonlocal operators, dual-support, operator energy functional, variational principle, Taylor series expansion, partial differential equations.

Nomenclature

Symbols	Description
$\boldsymbol{x}_i$	spatial coordinates in domain Ω
$\boldsymbol{u}$	displacement field
$\boldsymbol{\xi}_{ij}$	relative position vector
$\mathbb{w}(\boldsymbol{\xi}_{ij})$	the weight function
$\mathcal{S}_i$	the support of particle $\boldsymbol{x}_i$
$\mathcal{S}_i'$	the dual-support of particle $\boldsymbol{x}_i$
$\tilde{\nabla} \otimes \boldsymbol{u}_i$	nonlocal gradient operator of point $\boldsymbol{x}_i$
$\tilde{\nabla} \times \boldsymbol{u}_i$	nonlocal curl operator of point $\boldsymbol{x}_i$
$\tilde{\nabla} \cdot \boldsymbol{u}_i$	nonlocal divergence operator of point $\boldsymbol{x}_i$
$\mathcal{F}_i^{hg}$	operator energy functional of point $\boldsymbol{x}_i$
$\mathbf{K}_i$	the shape tensor
$\partial\Omega$	the boundary of domain Ω

$\boldsymbol{\sigma}$	Cauchy stress tensor
$\psi_e(\boldsymbol{\varepsilon}(\nabla \boldsymbol{u}), \phi)$	strain energy density
$\mathbf{b}$	the body force density
$\mathbf{f}$	the external traction force
ΔV_i	the volume associated with point $\boldsymbol{x}_i$
$\partial_\alpha^{\mathbb{1}} \mathbf{u}_i$	scaled partial derivatives
$\partial_\alpha \mathbf{u}_i$	partial derivatives
$\alpha_{\mathbb{r}}^{\mathbb{n}}$	multi-index notation
$\mathbf{B}_{\alpha i}$	the nonlocal operator coefficient matrix of point $\mathbf{x}_i$
$\boldsymbol{n}^*$	the outward-pointing normal vector for boundary $\partial\Omega_f$
$H(\mathbf{x}, T)$	the local history field of strain
G_c	the critical energy release rate
Abbreviations	**Description**
PDEs	Partial Differential Equations
NOM	Nonlocal Operator Method
FEM	Finite Element Method
XFEM	Extended Finite-Element Method
PG DEM	Petrov-Galerkin Diffuse Element Method
EFG	Element-Free Galerkin
RKPM	Reproducing Kernel Particle Method
PUM	Partition of Unity Methods
IGA	Isogeometric Analysis
GFDM	Generalized Finite Difference Method
SPH	Smoothed Particle Hydrodynamics
PD	Peridynamics
TSE	Taylor Series Expansion
PDDO	Peridynamic differential operator

1. Introduction

In engineering analysis, numerous central models can be quantitatively described by one or more partial differential equations (PDEs), known as the governing equations. PDEs describe complex phenomena such as motion, reaction, diffusion, equilibrium, conservation, just to name a few. Due to the complexity of most problems, analytical solutions exist only for restricted circumstances with simple geometries and boundary conditions. Therefore, numerical methods have been developed over many decades. They include the finite element method (FEM) [1]-[6], extended finite-element method (XFEM) [7, 8], Reproducing Kernel Particle Method (RKPM) [9]-[12], Petrov-Galerkin Diffuse Element Method (PG DEM) [13, 14], Partition of Unity Methods (PUM) [15]-[18], isogeometric analysis (IGA) [19]-[25], the reproducing kernel collocation method [26]-[33], Element-Free Galerkin (EFG) method [34]-[37], *hp*-Meshless clouds (HPC) [38], Generalized Finite Difference Method (GFDM) [39]-[43], Smoothed Particle Hydrodynamics (SPH) [44]-[48], Peridynamics (PD) [49], to name a few.

One key task in numerical methods for solving PDEs is to devise methodologies for numerically representing, formulating, and computing the various differential operators. In order to solve the unknown field, the FEM and most meshless methods, for example, employ shape functions by introducing interpolations or approximations of the field variables via nodal values. The shape function derivatives are then used to represent and compute the differential operators of the field variables. Or in other words, instead of applying the differential operators directly to the approximation, they are applied to the shape functions. In many applications, the construction of the shape functions and their derivatives can become challenging. Also problems with moving boundaries impose strong requirements on the shape functions of the underlying discretization. These issues can be dealt with meshless methods or so-called extended FEMs which employ enrichment functions and introduce additional degrees of freedom into the discretization. However, the implementation in 3D is challenging due to the description of the interface/frack topology.

Another efficient way to deal with such problems is to 'smear' out the discontinuity. So-called nonlocal theories introduce an intrinsic length scale and avoid treating problems with

discontinuities. They have been used nonlocal elasticity [50]-[54], nonlocal fluid dynamics [55]-[57], nonlocal continuum field theories [58]-[61], nonlocal electromagnetic theory [62]-[64], nonlocal damage mechanics [65]-[68] and nonlocal calculus [69, 70]. The nonlocal theory based on an integral form provides an improved predictive capability to capture effects that classical differential equations fail to capture. In comparison to the local theory, the nonlocal theory not only has a greater numerical well-posedness, but also resembles the real physical process better due to its inherent length scale [59, 71, 65]. A popular approach based on nonlocal theory is peridynamics (PD) [72]-[78], which has received great interest because of its comparatively simple numerical implementation for fracture. To account for long-range forces, PD reformulates the elasticity theory in integral form, overcoming the challenge of defining the local derivatives for fractures. In contrast to numerical models based on classical local continuum mechanics, PD theories employ integro-differential equations without displacement derivatives, which naturally enable the occurrence of discontinuities in the displacement field as it does not require spatial derivatives of the displacement field. Furthermore, PD can naturally deal with complicated fracture processes such as crack branching and coalescence. PD models include bond-based peridynamics (BB-PD) models [79]-[83], state-based peridynamic (SB-PD) models [84]-[89], dual-horizon peridynamics (DH-PD) [90]-[93] and hybrid models coupling classical continuum mechanics with PD [94]-[100]. PD has been applied to numerous problems such as plate/shell analysis [101]-[106], mixed peridynamic Petrov-Galerkin method [100, 107], phase-field damage models [108]-[111], wave dispersion analysis [112]-[117] and higher-order approaches [118]-[122], to name a few.

In recent years, several numerical approaches based on peridynamic differential operator (PDDO) [123]-[139] have been proposed, which can be viewed as an interesting extension of PD. PDDO employs the concept of PD interactions. It is based on the Taylor Series Expansion (TSE) of multi-variable scalar functions and the orthogonality property of PD functions. PDDO provides any order of derivatives to be derived directly from the orthogonality requirement of the PD functions without any differentiation. It does not use a kernel function or repeatability criteria for different derivative orders and permits the precise calculation of any arbitrary order of partial derivatives of spatial and temporal functions. Directly determining the PD functions for the derivatives is done by making them orthogonal to each term in the Taylor series expansion. When finding the PD functions in the presence of a nonsymmetric family, both the lower-order and higher-order derivatives affect each other. PDDO is exempt from the symmetric requirement which eliminates the need for ghost points at the boundary.

Another approach, which can be considered as an extension to PD, is the Nonlocal Operator Method (NOM), which has been first proposed in [140] for electromagnetic problems. The approach has been subsequently extended to mechanical problems in [141]-[150]. NOM is based on 'conventional' differential operators to define the nonlocal operators. It adopts concepts such as support and dual support with finite characteristic length, and it utilizes a TSE to calculate partial derivatives. NOM has been applied to numerous challenging problems in solid mechanics and is a viable alternative to FEM or meshless methods. In combination with the weighted residual and variational methodology, NOM constructs the operator energy functional through common matrix operations. While FEM and meshless methods require shape functions to compute derivatives, NOM acquires those through the differential operators 'naturally' without the use of shape functions. Or in other words: Nonlocal operators can be regarded as an alternative to partial derivatives of shape functions in FEM. The tangent stiffness is obtained naturally by simply defining an energy function, thus drastically simplifying the implementation. Since NOM also makes use of the concepts of support and dual-support, nonlocal strong forms for a wide range of physical problems can be naturally derived. Up to date, three versions of NOM have been presented: first-order / higher-order particle-based NOM and higher-order 'numerical integration-based' NOM. When nodal integration is used,

the particle-based version may be considered as a special case of NOM with numerical integration. In this paper, the developments and applications of NOM for solving PDEs are reviewed. The remainder of the paper is outlined as follows: In Section 2, we briefly review the NOM. Section 3 addresses applications of NOM for solving PDEs. Finally, some future research perspectives are presented in Section 4 before the manuscript concludes in Section 5.

2. Nonlocal operator method (NOM) and its developments

2.1. Fundamentals of NOM: Support, dual-support, nonlocal operators and operator energy functional

Consider the initial and present configurations of a solid, as depicted in Fig. 1(a). Let $\mathbf{x}_i$ be spatial coordinates in the domain $\boldsymbol{\Omega}$; the spatial vector $\boldsymbol{\xi}_{ij} := \mathbf{x}_j - \mathbf{x}_i$ starts from $\mathbf{x}_i$ to $\mathbf{x}_j$; $\mathbf{u}_i := \mathbf{u}(\mathbf{x}_i, t)$ and $\mathbf{u}_j := \mathbf{u}(\mathbf{x}_j, t)$ are the field values for $\mathbf{x}_i$ and $\mathbf{x}_j$, respectively; $\mathbf{u}_{ij} := \mathbf{u}_j - \mathbf{u}_i$ is the relative displacement field $\boldsymbol{\xi}_{ij}$ and **Support** $\mathcal{S}_i$ of point $\mathbf{x}_i$ is the domain where any spatial point $\mathbf{x}_j$ forms a spatial vector $\boldsymbol{\xi}_{ij}(= \mathbf{x}_j - \mathbf{x}_i)$ from $\mathbf{x}_i$ to $\mathbf{x}_j$. The support serves as the basis for the nonlocal operators. It should be noted there is no restriction on the support shapes (such as spherical, cube, and so on). **Dual-support** is defined as a union of the points whose supports include $\mathbf{x}$, indicated by

$$\mathcal{S}'_i = \{\mathbf{x}_j | \mathbf{x}_i \in \mathcal{S}_j\}. \tag{1}$$

Point $\mathbf{x}_j$ forms the dual-vector $\boldsymbol{\xi}'_{ij}(= \mathbf{x}_i - \mathbf{x}_j = -\boldsymbol{\xi}_{ij})$ in $\mathcal{S}'_i$; $\boldsymbol{\xi}'_{ij}$ is the spatial vector established in $\mathcal{S}_j$. Fig. 1(b) illustrates the concept of support and dual-support. NOM replaces the local operator with nonlocal operators. By substituting the local differential operator with the corresponding nonlocal operator, the functional defined by the local differential operator can be utilized to generate the residual or tangent stiffness matrix. The **nonlocal operators** for a

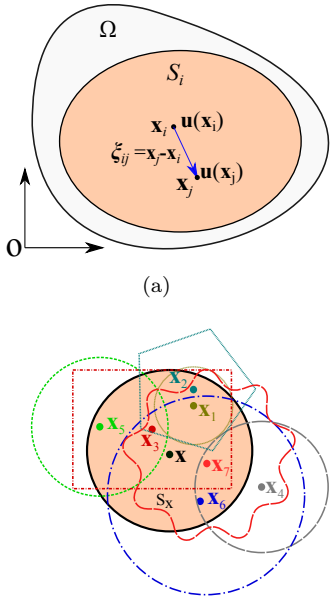

Fig. 1: (a) The deformed body configuration. (b) Support and dual-support schematic diagram, $\mathcal{S}_\mathbf{x} = \{\mathbf{x}_1, \mathbf{x}_2, \mathbf{x}_3, \mathbf{x}_5, \mathbf{x}_6, \mathbf{x}_7\}$, $\mathcal{S}'_\mathbf{x} = \{\mathbf{x}_3, \mathbf{x}_6, \mathbf{x}_7\}$.

vector field $\mathbf{u}$ and scalar field u for point $\mathbf{x}_i$ in support $\mathcal{S}_i$ can be defined as follows

1 Nonlocal gradient operator

$$\begin{cases} \text{(a) Vector field} \quad \tilde{\nabla} \otimes \mathbf{u}_i := \\ \displaystyle\int_{\mathcal{S}_i} \mathrm{w}(\boldsymbol{\xi}_{ij}) \mathbf{u}_{ij} \otimes \boldsymbol{\xi}_{ij} \mathrm{d}V_j \cdot \Big(\int_{\mathcal{S}_i} \mathrm{w}(\boldsymbol{\xi}_{ij}) \boldsymbol{\xi}_{ij} \otimes \boldsymbol{\xi}_{ij} \mathrm{d}V_j \Big)^{-1} \\ \text{(b) Scalar field} \quad \tilde{\nabla} u_i := \\ \displaystyle\int_{\mathcal{S}_i} \mathrm{w}(\boldsymbol{\xi}_{ij}) u_{ij} \boldsymbol{\xi}_{ij} \mathrm{d}V_j \cdot \Big(\int_{\mathcal{S}_i} \mathrm{w}(\boldsymbol{\xi}_{ij}) \boldsymbol{\xi}_{ij} \otimes \boldsymbol{\xi}_{ij} \mathrm{d}V_j \Big)^{-1} \end{cases} \tag{2}$$

2 Nonlocal curl operator

$$\text{Vector field} \quad \tilde{\nabla} \times \mathbf{u}_i := \int_{\mathcal{S}_i} \mathrm{w}(\boldsymbol{\xi}_{ij}) \Big(\big(\int_{\mathcal{S}_i} \mathrm{w}(\boldsymbol{\xi}_{ij}) \boldsymbol{\xi}_{ij} \otimes \boldsymbol{\xi}_{ij} \mathrm{d}V_j \big)^{-1} \cdot \boldsymbol{\xi}_{ij} \Big) \times \mathbf{u}_{ij} \mathrm{d}V_j \tag{3}$$

3 Nonlocal divergence operator

$$\text{Vector field} \quad \tilde{\nabla} \cdot \mathbf{u}_i := \int_{\mathcal{S}_i} \mathrm{w}(\boldsymbol{\xi}_{ij}) \mathbf{u}_{ij} \cdot \Big(\big(\int_{\mathcal{S}_i} \mathrm{w}(\boldsymbol{\xi}_{ij}) \boldsymbol{\xi}_{ij} \otimes \boldsymbol{\xi}_{ij} \mathrm{d}V_j \big)^{-1} \cdot \boldsymbol{\xi}_{ij} \Big) \mathrm{d}V_j \tag{4}$$

The **operator energy functional** for a vector field $\mathbf{u}$ and scalar field u for point $\mathbf{x}_i$ in support $\mathcal{S}_i$ can be defined as follows

$$\begin{cases} \text{(a) Vector field} \\ \mathcal{F}_i^{hg} = \dfrac{p^{hg}}{2m_{\mathbf{K}_i}} \displaystyle\int_{\mathcal{S}_i} \mathbb{w}(\boldsymbol{\xi}_{ij})(\tilde{\nabla}\mathbf{u}_i \cdot \boldsymbol{\xi}_{ij} - \mathbf{u}_{ij})^T \\ \qquad\qquad (\tilde{\nabla}\mathbf{u}_i \cdot \boldsymbol{\xi}_{ij} - \mathbf{u}_{ij})\mathrm{d}V_j \\ \text{(b) Scalar field} \\ \mathcal{F}_i^{hg} = \dfrac{p^{hg}}{2m_{\mathbf{K}_i}} \displaystyle\int_{\mathcal{S}_i} \mathbb{w}(\boldsymbol{\xi}_{ij})(\tilde{\nabla}u_i\boldsymbol{\xi}_{ij} - u_{ij}) \\ \qquad\qquad (\tilde{\nabla}u_i\boldsymbol{\xi}_{ij} - u_{ij})\mathrm{d}V_j \end{cases} \tag{5}$$

where $\mathbb{w}(\boldsymbol{\xi}_{ij})$ is the weight function, $\frac{p^{hg}}{2m_{\mathbf{K}_i}}$ is a coefficient for the operator energy functional, p^{hg} is the penalty coefficient, $m_{\mathbf{K}_i}(=\mathrm{tr}[\mathbf{K}_i])$ is the normalization coefficient and $\mathbf{K}_i$ is a shape tensor defined as

$$\mathbf{K}_i = \int_{\mathcal{S}_i} \mathbb{w}(\boldsymbol{\xi}_{ij})\boldsymbol{\xi}_{ij} \otimes \boldsymbol{\xi}_{ij}\mathrm{d}V_j \tag{6}$$

2.2. First-order particle-based NOM

The first-order NOM was proposed for the solution of PDEs by Rabczuk, et al. [140, 141]. In the first-order particle-based NOM, a vector field $\mathbf{u}$ at a point (0,0) is approximated by using a Taylor series expansion neglecting higher order terms

$$\mathbf{u}' = \mathbf{u} + \nabla\mathbf{u} \cdot \boldsymbol{\xi} + O(\boldsymbol{\xi}^2) \tag{7}$$

where $\nabla := (\frac{\partial}{\partial x}, \frac{\partial}{\partial y}, \frac{\partial}{\partial z})^T$, $\boldsymbol{\xi} := (x, y, z)^T$ denotes the initial bond vector, $O(\boldsymbol{\xi}^2)$ represents higher order terms, and for a linear field $O(\boldsymbol{\xi}^2) = 0$. The nonlocal gradient operator $\tilde{\nabla}\mathbf{u}_i$ at point $\mathbf{x}_i$ is written as

$$\tilde{\nabla}\mathbf{u}_i = \sum_{j\in\mathcal{S}_i} \mathbb{w}\left(\boldsymbol{\xi}_{ij}\right)\left(\mathbf{u}_j - \mathbf{u}_i\right) \otimes \boldsymbol{\xi}_{ij}\Delta V_j \cdot \left[\sum\nolimits_j \mathbb{w}\left(\boldsymbol{\xi}_{ij}\right)\boldsymbol{\xi}_{ij} \otimes \boldsymbol{\xi}_{ij}\Delta V_j\right]^{-1} \tag{8}$$

The matrix form of the nonlocal gradient operator $\tilde{\nabla}\mathbf{u}$ at point $\mathbf{x}_i$ for a vector field can be written as

$$\begin{aligned} \tilde{\nabla}\mathbf{u}_i &= \begin{bmatrix} \frac{\partial u_i}{\partial x} & \frac{\partial u_i}{\partial y} & \frac{\partial u_i}{\partial z} \\ \frac{\partial v_i}{\partial x} & \frac{\partial v_i}{\partial y} & \frac{\partial v_i}{\partial z} \\ \frac{\partial w_i}{\partial x} & \frac{\partial w_i}{\partial y} & \frac{\partial w_i}{\partial z} \end{bmatrix} \\ &= \begin{bmatrix} -\sum_{j\in\mathcal{S}_i}\xi_{x_j} & \xi_{x_{j1}} & \cdots & \xi_{x_{jn}} \\ -\sum_{j\in\mathcal{S}_i}\xi_{y_j} & \xi_{y_{j1}} & \cdots & \xi_{y_{jn}} \\ -\sum_{j\in\mathcal{S}_i}\xi_{z_j} & \xi_{z_{j1}} & \cdots & \xi_{z_{jn}} \end{bmatrix} \begin{bmatrix} u_i & v_i & w_i \\ u_{j1} & v_{j1} & w_{j1} \\ \cdots & \cdots & \cdots \\ u_{jn} & v_{jn} & w_{jn} \end{bmatrix} \end{aligned} \tag{9}$$

The matrix form of the nonlocal gradient operator can be transformed to vector field $\tilde{\nabla}\mathbf{u}_i$ given as

$$\begin{aligned} \tilde{\nabla}\mathbf{u}_i &= \left[\frac{\partial u_i}{\partial x}, \frac{\partial u_i}{\partial y}, \frac{\partial u_i}{\partial z}, \frac{\partial v_i}{\partial x}, \frac{\partial v_i}{\partial y}, \frac{\partial v_i}{\partial z}, \frac{\partial w_i}{\partial x}, \frac{\partial w_i}{\partial y}, \frac{\partial w_i}{\partial z}\right]^T \\ &= \mathscr{B}_i\mathscr{U}_i, \end{aligned} \tag{10}$$

where $\mathscr{B}_i :=$

$$\begin{bmatrix} -\sum_{j\in\mathcal{S}_i}\xi_{x_j} & 0 & 0 & \xi_{x_{j1}} & 0 & 0 & \cdots & \xi_{x_{jn}} & 0 & 0 \\ 0 & -\sum_{j\in\mathcal{S}_i}\xi_{y_j} & 0 & 0 & \xi_{y_{j1}} & 0 & \cdots & 0 & \xi_{y_{jn}} & 0 \\ 0 & 0 & -\sum_{j\in\mathcal{S}_i}\xi_{z_j} & 0 & 0 & \xi_{z_{j1}} & \cdots & 0 & 0 & \xi_{z_{jn}} \\ -\sum_{j\in\mathcal{S}_i}\xi_{x_j} & 0 & 0 & \xi_{x_{j1}} & 0 & 0 & \cdots & \xi_{x_{jn}} & 0 & 0 \\ 0 & -\sum_{j\in\mathcal{S}_i}\xi_{y_j} & 0 & 0 & \xi_{y_{j1}} & 0 & \cdots & 0 & \xi_{y_{jn}} & 0 \\ 0 & 0 & -\sum_{j\in\mathcal{S}_i}\xi_{z_j} & 0 & 0 & \xi_{z_{j1}} & \cdots & 0 & 0 & \xi_{z_{jn}} \\ -\sum_{j\in\mathcal{S}_i}\xi_{x_j} & 0 & 0 & \xi_{x_{j1}} & 0 & 0 & \cdots & \xi_{x_{jn}} & 0 & 0 \\ 0 & -\sum_{j\in\mathcal{S}_i}\xi_{y_j} & 0 & 0 & \xi_{y_{j1}} & 0 & \cdots & 0 & \xi_{y_{jn}} & 0 \\ 0 & 0 & -\sum_{j\in\mathcal{S}_i}\xi_{z_j} & 0 & 0 & \xi_{z_{j1}} & \cdots & 0 & 0 & \xi_{z_{jn}} \end{bmatrix};$$

$$\mathscr{U}_i := \left[u_i, v_i, w_i, u_{j1}, v_{j1}, w_{j1}, \cdots, u_{jn}, v_{jn}, w_{jn}\right]^T$$

The nonlocal gradient operator $\tilde{\nabla}u$ at point $\mathbf{x}_i$ for a scalar field is written as

$$\begin{aligned} \tilde{\nabla}u_i &= \begin{bmatrix} \frac{\partial u_i}{\partial x} \\ \frac{\partial u_i}{\partial y} \\ \frac{\partial u_i}{\partial z} \end{bmatrix} \\ &= \begin{bmatrix} -\sum_{j\in\mathcal{S}_i}\xi_{x_j} & \xi_{x_{j1}} & \cdots & \xi_{x_{jn}} \\ -\sum_{j\in\mathcal{S}_i}\xi_{y_j} & \xi_{y_{j1}} & \cdots & \xi_{y_{jn}} \\ -\sum_{j\in\mathcal{S}_i}\xi_{z_j} & \xi_{z_{j1}} & \cdots & \xi_{z_{jn}} \end{bmatrix} \begin{bmatrix} u_i \\ u_{j1} \\ \cdots \\ u_{jn} \end{bmatrix} \\ &=: \mathscr{B}_i\mathscr{U}_i \end{aligned} \tag{11}$$

with

$$\left(\xi_{x_j}, \xi_{y_j}, \xi_{z_j}\right) = \mathbb{w}\left(\boldsymbol{\xi}_{ij}\right)\boldsymbol{\xi}_{ij}^T V_j \cdot \left[\sum_{j\in\mathcal{S}_i} \mathbb{w}\left(\boldsymbol{\xi}_{ij}\right)\boldsymbol{\xi}_{ij} \otimes \boldsymbol{\xi}_{ij}\Delta V_j\right]^{-1}$$

Nodal integration, which is commonly used in the NOM, suffers from a zero-energy mode [151, 152], which in turn results in numerical

instability. To eliminate these instabilities, traditional PD and SPH introduce a penalty term to the force state [153]. However, this approach is only applicable for explicit dynamics. NOM on the other hand employs the operator energy functional to prevent numerical instabilities. In first-order NOM, the operator energy functional and its tangent stiffness matrix can be written as [141, 149]

$$\mathcal{F}_i^{hg} = \frac{p^{hg}}{2m_{\mathbf{K}_i}} \mathscr{U}_i{}^T \left(\begin{bmatrix} \sum_{j\in\mathcal{S}_i} \mathbf{I}_j & -\mathbf{I}_{j1} & \cdots & -\mathbf{I}_{jn} \\ -\mathbf{I}_{j1} & \mathbf{I}_{j1} & \mathbf{0} & \mathbf{0} \\ \vdots & \mathbf{0} & \ddots & \mathbf{0} \\ -\mathbf{I}_{jn} & \mathbf{0} & \mathbf{0} & \mathbf{I}_{jn} \end{bmatrix} - \mathscr{B}_i{}^T \begin{bmatrix} \mathbf{K}_i & 0 & 0 \\ 0 & \mathbf{K}_i & 0 \\ 0 & 0 & \mathbf{K}_i \end{bmatrix} \mathscr{B}_i \right) \mathscr{U}_i \quad (12)$$

where $\mathbf{I}_j = \mathbb{w}(\boldsymbol{\xi}_{ij})\Delta V_j(1,1,1) \otimes (1,1,1)^T$.

$$\mathscr{K}_i^{hg} = \frac{p^{hg}}{m_{\mathbf{K}_i}} \left(\begin{bmatrix} \sum_{j\in\mathcal{S}_i} \mathbf{I}_j & -\mathbf{I}_{j1} & \cdots & -\mathbf{I}_{jn} \\ -\mathbf{I}_{j1} & \mathbf{I}_{j1} & \mathbf{0} & \mathbf{0} \\ \vdots & \mathbf{0} & \ddots & \mathbf{0} \\ -\mathbf{I}_{jn} & \mathbf{0} & \mathbf{0} & \mathbf{I}_{jn} \end{bmatrix} - \mathscr{B}_i{}^T \begin{bmatrix} \mathbf{K}_i & 0 & 0 \\ 0 & \mathbf{K}_i & 0 \\ 0 & 0 & \mathbf{K}_i \end{bmatrix} \mathscr{B}_i \right) \quad (13)$$

The global tangent stiffness matrix in support $\mathcal{S}_i$ can be expressed as

$$\mathbb{K}_i = \sum_{j\in\mathcal{S}_i} \left(\mathscr{B}_i{}^T \Big(\mathscr{D} - \frac{p^{hg}}{m_{\mathbf{K}_i}} \begin{bmatrix} \mathbf{K}_i & 0 & 0 \\ 0 & \mathbf{K}_i & 0 \\ 0 & 0 & \mathbf{K}_i \end{bmatrix} \Big) \mathscr{B}_i + \frac{p^{hg}}{m_{\mathbf{K}_i}} \begin{bmatrix} \sum_{j\in\mathcal{S}_i} \mathbf{I}_j & -\mathbf{I}_{j1} & \cdots & -\mathbf{I}_{jn} \\ -\mathbf{I}_{j1} & \mathbf{I}_{j1} & \mathbf{0} & \mathbf{0} \\ \vdots & \mathbf{0} & \ddots & \mathbf{0} \\ -\mathbf{I}_{jn} & \mathbf{0} & \mathbf{0} & \mathbf{I}_{jn} \end{bmatrix} \right) \Delta V_j \quad (14)$$

2.3. Higher order particle-based NOM

The first-order particle-based NOM [140, 141] can solve lower order (up to fourth-order) PDEs, but their accuracy degrades considerably as the order of the PDE increases. Therefore, a higher-order NOM has been proposed in [142], which is applicable to the solution of higher-order PDEs of any order, including coupled problems. The higher-order NOM acquires all partial derivatives of higher orders in a straightforward and efficient manner without the need for shape functions as stated before. Independent of the numerical implementation, it can be utilized to establish nonlocal governing equations based on the energy functional. In the higher-order particle-based NOM, a vector field $\mathbf{u}$ at a point $\mathbf{x}_j \in \mathcal{S}_i$ is approximated by using a vector form of the Taylor series expansion that includes the characteristic length scale $\mathbb{l}_i$ of support $\mathcal{S}_i$ at $\mathbf{u}_i$ in dimensions with $\mathbb{n}$ as the highest order of derivatives:

$$\mathbf{u}_j = \mathbf{u}_i + \sum_{(\mathbb{n}_1,\ldots,\mathbb{n}_\mathbb{r})\in\alpha_\mathbb{r}^\mathbb{n}} \frac{\boldsymbol{\xi}_1^{\mathbb{n}_1}\ldots\boldsymbol{\xi}_\mathbb{r}^{\mathbb{n}_\mathbb{r}}}{\mathbb{l}_i^{\mathbb{n}_1+\ldots+\mathbb{n}_\mathbb{r}}} \left(\frac{\mathbb{l}_i^{\mathbb{n}_1+\ldots+\mathbb{n}_\mathbb{r}}}{\mathbb{n}_1!\ldots\mathbb{n}_\mathbb{r}!} u_{i,\mathbb{n}_1\ldots\mathbb{n}_\mathbb{r}} \right) + O(\boldsymbol{\xi}^{\mathbb{n}+1}) \quad (15)$$

where $\alpha_\mathbb{r}^\mathbb{n}$ is the list of flattened multi-indices, $\mathbb{l}_i$ is a characteristic length of support $\mathcal{S}_i$ at $\mathbf{u}_i$ and the factor can be written as

$$\alpha_\mathbb{r}^\mathbb{n} = \{(\mathbb{n}_1,\ldots,\mathbb{n}_\mathbb{r}) | 1 \le \sum_{i=1}^{\mathbb{r}} \mathbb{n}_i \le \mathbb{n}, \mathbb{n}_i \in \mathbb{N}^0, 1 \le i \le \mathbb{r}\} \quad (16)$$

$$\boldsymbol{\xi}_{ij} = (\mathbf{x}_{j1} - \mathbf{x}_{i1}, \ldots, \mathbf{x}_{jd} - \mathbf{x}_{id}) \quad (17)$$

$$\mathbf{u}_{i,\mathbb{n}_1\ldots\mathbb{n}_\mathbb{r}} = \frac{\partial^{\mathbb{n}_1+\ldots+\mathbb{n}_\mathbb{r}}\mathbf{u}_i}{\partial\mathbf{x}_{i1}^{\mathbb{n}_1}\ldots\partial\mathbf{x}_{id}^{\mathbb{n}_\mathbb{r}}} \quad (18)$$

$$|\alpha| = \max(\mathbb{n}_1 + \ldots + \mathbb{n}_\mathbb{r}) \quad (19)$$

The list of the flattened polynomials $\boldsymbol{p}_j^\mathbb{l}$, scaled partial derivatives $\partial_\alpha^\mathbb{l}\mathbf{u}_i$ and partial derivatives $\partial_\alpha\mathbf{u}_i$ in higher NOM are written as

$$\begin{aligned} \boldsymbol{p}_j^\mathbb{l} &= (\frac{\boldsymbol{\xi}_\mathbb{r}}{\mathbb{l}}, \ldots, \frac{\boldsymbol{\xi}_1^{\mathbb{n}_1}\ldots\boldsymbol{\xi}_\mathbb{r}^{\mathbb{n}_\mathbb{r}}}{\mathbb{l}^{\mathbb{n}_1+\ldots+\mathbb{n}_\mathbb{r}}}, \ldots, \frac{\boldsymbol{\xi}_1^\mathbb{n}}{\mathbb{l}^\mathbb{n}})^T \\ \partial_\alpha^\mathbb{l}\mathbf{u}_i &= (\mathbf{u}_{i,0\ldots1}^\mathbb{l}, \ldots, \mathbf{u}_{i,\mathbb{n}_1\ldots\mathbb{n}_\mathbb{r}}^\mathbb{l}, \ldots, \mathbf{u}_{i,\mathbb{n}\ldots0}^\mathbb{l})^T \\ \partial_\alpha\mathbf{u}_i &= (\mathbf{u}_{i,0\ldots1}, \ldots, \mathbf{u}_{i,\mathbb{n}_1\ldots\mathbb{n}_\mathbb{r}}, \ldots, \mathbf{u}_{i,\mathbb{n}\ldots0})^T. \end{aligned} \quad (20)$$

The nonlocal operator $\tilde{\partial}_\alpha\mathbf{u}_i$ at point $\mathbf{x}_i$ is given by

$$\begin{aligned} \tilde{\partial}_\alpha\mathbf{u}_i &= \mathbb{L}_i^{-1} \Big(\int_{\mathcal{S}_i} \mathbb{w}(\boldsymbol{\xi}_{ij}) \boldsymbol{p}_j^\mathbb{l} \otimes (\boldsymbol{p}_j^\mathbb{l})^T \mathrm{d}V_j \Big)^{-1} \cdot \int_{\mathcal{S}_i} \mathbb{w}(\boldsymbol{\xi}_{ij}) \boldsymbol{p}_j^\mathbb{l} \mathbf{u}_{ij} \mathrm{d}V_j \\ &= \mathbf{K}_{\alpha i} \boldsymbol{p}_{\mathbb{w}i}^\mathbb{l} \Delta\mathbf{u}_i \end{aligned} \quad (21)$$

where

$$\mathbb{L}_i = \mathrm{diag}\big[\mathbb{l}_i, ..., \frac{\mathbb{l}_i^{\mathrm{n}_1+...+\mathrm{n}_\mathrm{r}}}{\mathrm{n}_1!...\mathrm{n}_\mathrm{r}!}, ..., \frac{\mathbb{l}_i^{\mathrm{n}}}{\mathrm{n}!}\big] \tag{22}$$

$$\boldsymbol{p}^{\mathbb{l}}_{\mathrm{w}i} = \Big(\mathrm{w}(\boldsymbol{\xi}_{ij_1})\boldsymbol{p}^{\mathbb{l}}_{j_1}\Delta V_{j_1}, ..., \mathrm{w}(\boldsymbol{\xi}_{ij_{n_i}})\boldsymbol{p}^{\mathbb{l}}_{j_{n_i}}\Delta V_{j_{n_i}}\Big) \tag{23}$$

$$\Delta\mathbf{u}_i = (\mathbf{u}_{ij_1}, ..., \mathbf{u}_{ij_k}, ..., \mathbf{u}_{ij_n})^T \tag{24}$$

The matrix form of the nonlocal operator $\tilde{\partial}_\alpha\mathbf{u}_i$ is

$$\begin{aligned}\tilde{\partial}_\alpha\mathbf{u}_i &= \mathbf{K}_{\alpha i}\boldsymbol{p}^{\mathbb{l}}_{\mathrm{w}i}\Delta\mathbf{u}_i \\ &= \big[-(1,\cdots,1)_n\mathbf{K}_{\alpha i}\mathbf{p}^{\mathbb{l}}_{\mathrm{w}i}, \mathbf{K}_{\alpha i}\mathbf{p}^{\mathbb{l}}_{\mathrm{w}i}\big]\begin{bmatrix}\mathbf{u}_i\\ \mathbf{u}_{j_1}\\ \mathbf{u}_{j_2}\\ \cdots\\ \mathbf{u}_{j_n}\end{bmatrix} \\ &=: \mathbf{B}_{\alpha i}\mathbf{U}_i\end{aligned} \tag{25}$$

where $\mathbf{B}_{\alpha i}$ is the nonlocal operator coefficient matrix of point $\mathbf{x}_i$, $(1,\cdots,1)_{n_p}\mathbf{K}_{\alpha i}\mathbf{p}^{\mathbb{l}}_{\mathrm{w}i}$ is the column sum of $\mathbf{K}_{\alpha i}\mathbf{p}^{\mathbb{l}}_{\mathrm{w}i}$. The operator energy functional can be expressed by

$$\mathcal{F}^{hg}_{\alpha i} = \frac{p^{hg}}{2m_{\mathbf{K}_i}}\sum_{j\in\mathcal{S}_i}\mathrm{w}(\boldsymbol{\xi}_{ij})\big(\mathbf{u}_{ij} - (\boldsymbol{p}^{\mathbb{l}}_j)^T\tilde{\partial}^{\mathbb{l}}_\alpha\mathbf{u}_i\big)^2\Delta V_j \tag{26}$$

The quadratic operator energy functional can be simplified into

$$\begin{aligned}\mathcal{F}^{hg}_{\alpha i} =& \frac{p^{hg}}{2m_{\mathbf{K}_i}}(\mathbf{K}^{-1}_{\alpha i}\mathbf{p}^{\mathbb{l}}_{\mathrm{w}i}\mathbf{B}_{\alpha i}\mathbf{U}_i)^T\Big(\begin{bmatrix}\mathbf{I}_{j1} & \mathbf{0} & \mathbf{0}\\ \mathbf{0} & \ddots & \mathbf{0}\\ \mathbf{0} & \mathbf{0} & \mathbf{I}_{j_n}\end{bmatrix} \\ &- (\boldsymbol{p}^{\mathbb{l}}_{\mathrm{w}i})^T\mathbf{K}_i\mathbb{L}_i\boldsymbol{p}^{\mathbb{l}}_{\mathrm{w}i}\Big)\mathbf{K}^{-1}_{\alpha i}\mathbf{p}^{\mathbb{l}}_{\mathrm{w}i}\mathbf{B}_{\alpha i}\mathbf{U}_i\end{aligned} \tag{27}$$

where $\mathbf{I}_j = \mathrm{w}(\boldsymbol{\xi}_{ij})\Delta V_j(1,1,1)\otimes(1,1,1)^T$. The tangent stiffness matrix caused by operator energy functional is written as

$$\begin{aligned}\mathscr{K}^{hg}_{\alpha i} =& \frac{p^{hg}}{m_{\mathbf{K}_i}}(\mathbf{K}^{-1}_{\alpha i}\mathbf{p}^{\mathbb{l}}_{\mathrm{w}i}\mathbf{B}_{\alpha i})^T\Big(\begin{bmatrix}\mathbf{I}_{j1} & \mathbf{0} & \mathbf{0}\\ \mathbf{0} & \ddots & \mathbf{0}\\ \mathbf{0} & \mathbf{0} & \mathbf{I}_{j_n}\end{bmatrix} \\ &- (\boldsymbol{p}^{\mathbb{l}}_{\mathrm{w}i})^T\mathbf{K}_{\alpha i}\mathbb{L}_i\boldsymbol{p}^{\mathbb{l}}_{\mathrm{w}i}\Big)\mathbf{K}^{-1}_{\alpha i}\mathbf{p}^{\mathbb{l}}_{\mathrm{w}i}\mathbf{B}_{\alpha i}\end{aligned} \tag{28}$$

The global tangent stiffness matrix in support $\mathcal{S}_i$ can be expressed as

$$\begin{aligned}\mathbb{K}_{\alpha i} = \sum_{j\in\mathcal{S}_i}\Bigg(&\mathbf{B}_{\alpha i}{}^T\cdot\mathscr{D}\cdot\mathbf{B}_{\alpha i} \\ &+ \frac{p^{hg}}{m_{\mathbf{K}_i}}(\mathbf{K}^{-1}_{\alpha i}\mathbf{p}^{\mathbb{l}}_{\mathrm{w}i}\mathbf{B}_{\alpha i})^T\Big(\begin{bmatrix}\mathbf{I}_{j1} & \mathbf{0} & \mathbf{0}\\ \mathbf{0} & \ddots & \mathbf{0}\\ \mathbf{0} & \mathbf{0} & \mathbf{I}_{j_n}\end{bmatrix} \\ &- (\boldsymbol{p}^{\mathbb{l}}_{\mathrm{w}i})^T\mathbf{K}_{\alpha i}\mathbb{L}_i\boldsymbol{p}^{\mathbb{l}}_{\mathrm{w}i}\Big)\mathbf{K}^{-1}_{\alpha i}\mathbf{p}^{\mathbb{l}}_{\mathrm{w}i}\mathbf{B}_{\alpha i}\Bigg)\Delta V_j\end{aligned} \tag{29}$$

2.4. Higher-order 'numerical integration-based' NOM

The particle-based first-order and higher-order NOM have difficulties in precisely enforcing boundary conditions of arbitrary order decreasing the convergence rate. Furthermore, particle-based approaches need stabilization, which can be accomplished, for example, using the operator energy functional [140]-[142]. Nevertheless, the operator energy functional contains a penalty factor. Ren et al. [143] proposed a scheme with approximation property, which specifies partial derivatives of various orders at a point by the nodes in the support and employs a background mesh for numerical integration, which circumvents just mentioned restrictions. A modified variational principle is used to impose the boundary conditions. When nodal integration is utilized, the particle-based NOM can be considered as a specific version of 'NOM with approximation property'. The numerical integration methodology considerably increases the method's stability. As a result, the operator energy functional needed in the particle-based NOM is avoided. However, the NOM approximation scheme does not meet the Kronecker-delta property, which makes the enforcement of Dirichlet boundary requirements problematic. Dirichlet boundary conditions can be enforced in a variety of ways in meshless methods. The penalty method, the Lagrange multiplier method and the modified variational principle are among the most prevalent schemes. To impose the boundary requirements, the modified variational principle is adopted here. Thus,

the energy functional is divided into two components that are connected to the domain and the boundary:

$$\mathcal{F} = \int_{\Omega} \mathbb{f} \mathrm{d}\Omega + \sum_{i} \int_{\Gamma_i} \bar{\mathbb{f}}_i \mathrm{d}\Gamma \tag{30}$$

where $\mathbb{f}$ is the energy functionals defined in the domain, $\bar{\mathbb{f}}_i$ is the functionals defined on the boundaries. In most cases, the boundary functional is more complicated than that in the domain. The residual vector and tangent stiffness matrix can be derived when combined with the nonlocal operator matrix.

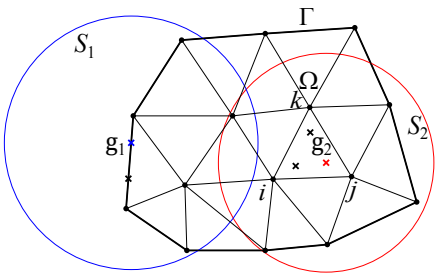

Fig. 2: Schematic diagram of supports for integration points in the domain and on the boundary [143].

Gauss quadrature based on a tetrahedra background mesh is employed. The linear tetrahedron's integration point is represented in terms of local coordinates (ξ, η, ζ). The integration point's global coordinate can be determined as

$$(x, y, z) = \sum_{j=1}^{4} N_j(\xi, \eta, \zeta)\,(x_j, y_j, z_j) \tag{31}$$

where (x_j, y_j, z_j) are the element's j-th nodal coordinates and N_j is the shape function of the four-node tetrahedron. The integration point's weight is

$$w = w_c |\boldsymbol{J}| = w_c \begin{vmatrix} \frac{\partial x}{\partial \xi} & \frac{\partial y}{\partial \xi} & \frac{\partial z}{\partial \xi} \\ \frac{\partial x}{\partial \eta} & \frac{\partial y}{\partial \eta} & \frac{\partial z}{\partial \eta} \\ \frac{\partial x}{\partial \zeta} & \frac{\partial y}{\partial \zeta} & \frac{\partial z}{\partial \zeta} \end{vmatrix} \tag{32}$$

where w_c is the weighted coefficient.

It should be emphasized that the background mesh is just necessary for integration, and NOM does not require the FE shape function derivatives. As a result, the shape functions of low-order elements are adequate for solving higher-order PDEs. The support domain of each integration point in the higher-order 'numerical integration-based' NOM is established by neighboring nodes instead of the integration points. The node-set acts as an approximation scheme for each Gauss point. However, dual-support is not necessary for integration points because they do not support any other nodes.

3. Applications of NOM for solving PDEs

3.1. Maxwell's equations

Maxwell's equations (Tab. 1) [154]-[158] are a set of coupled partial differential equations that lay the basis of classical electromagnetism, optics and electromagnetism. They describe how charges, currents and field changes create electric and magnetic fields.

Maxwell electromagnetic waveguide problems have been solved by many computational methods such as FEM [159], the method of moments [160], time domain finite difference method [161], ray theory [162], meshless/meshfree methods [163, 164], asymptotic-expansion methods [165] and eigen expansion method [166]. Rabczuk et al. [140] first proposed a NOM based on the variational principle for Maxwell electromagnetic waveguide problems as shown in Fig. 3 and Tab. 2.

The nonlocal formulation facilitates the assembly of the tangent stiffness matrix, which is critical for the waveguide problem's eigenvalue analysis. Case 2 has a frequency inaccuracy of less than 4%. The numerical and theoretical results are in good agreement.

3.2. Nonhomogeneous biharmonic equation

The biharmonic equation [167]-[170] is a fourth-order PDE important for instance for plate/shell theory [171]-[175]. It is particularly useful in

Tab. 1: Maxwell's equations in SI units form [158, 159].

Name	Integral equations	Differential equations
Gauss's law	$\oiint_{\partial\Omega} \mathbf{E}\cdot\mathrm{d}\mathbf{S} = \frac{1}{\varepsilon_0}\iiint_{\Omega}\rho\mathrm{d}V$	$\nabla\cdot\mathbf{E} = \frac{\rho}{\varepsilon_0}$
Gauss's law for magnetism	$\oiint_{\partial\Omega} \mathbf{B}\cdot\mathrm{d}\mathbf{S} = 0$	$\nabla\cdot\mathbf{B} = 0$
Maxwell-Faraday equation (Faraday's law of induction)	$\oint_{\partial\Sigma} \mathbf{E}\cdot\mathrm{d}\boldsymbol{\ell} = -\frac{\mathrm{d}}{\mathrm{d}t}\iint_{\Sigma}\mathbf{B}\cdot\mathrm{d}\mathbf{S}$	$\nabla\times\mathbf{E} = -\frac{\partial\mathbf{B}}{\partial t}$
Ampère's circuital law (with Maxwell's addition)	$\oint_{\partial\Sigma} \mathbf{B}\cdot\mathrm{d}\boldsymbol{\ell} = \mu_0\left(\iint_{\Sigma}\mathbf{J}\cdot\mathrm{d}\mathbf{S} + \varepsilon_0\frac{\mathrm{d}}{\mathrm{d}t}\iint_{\Sigma}\mathbf{E}\cdot\mathrm{d}\mathbf{S}\right)$	$\nabla\times\mathbf{B} = \mu_0\left(\mathbf{J} + \varepsilon_0\frac{\partial\mathbf{E}}{\partial t}\right)$

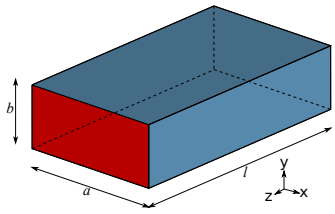

(a) Set up of rectangular waveguide ($22.86 \times 10.16 \times 40mm^3$)

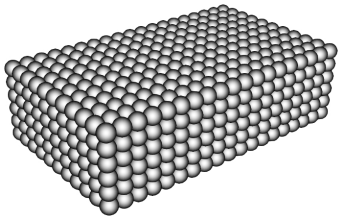

(b) Case 1: $11 \times 6 \times 19$

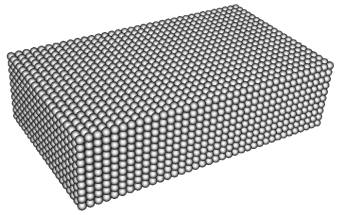

(c) Case 2: $21 \times 10 \times 36$

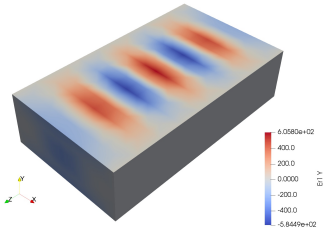

(d) Case 1: TE10

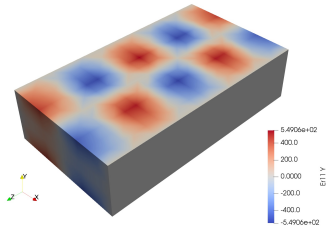

(e) Case 1: TE20

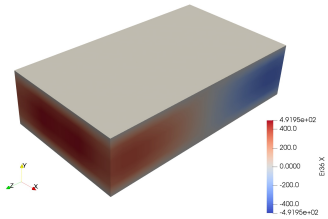

(f) Case 1: TE01

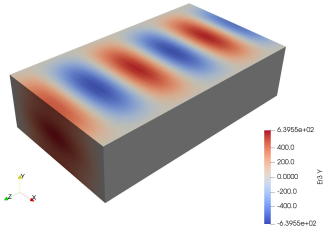

(g) Case 2: TE10

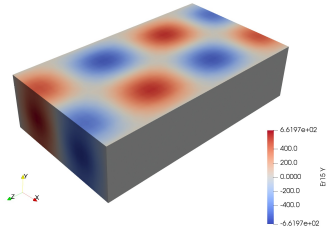

(h) Case 2: TE20

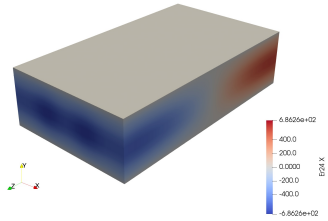

(i) Case 2: TE01

Fig. 3: The setup of rectangular waveguide (a), the discretizations for two cases (b-c); the TE modes for case 1(d-f) and case 2(g-i) [140].

modeling thin structures. It can be written as

$$\nabla^4 w = 0 \tag{33}$$

where ∇^4 is the fourth order ∇ operator and the square of the Laplacian operator ∇^2 (or Δ) is the biharmonic or bilaplacian operator. It can be expressed in n dimensions Cartesian coordi-

Tab. 2: Comparison of $f_{c_{mn}}$ between NOM results and exact results [140].

Mode	TE_{10}(GHz)	TE_{20} (GHz)	TE_{01} (GHz)
Case 1	6.02(-8.29%)	12.33(-5.28%)	15.08(3.13%)
Case 2	6.30(-3.96%)	12.67(-2.67%)	14.91(1.88%)
Exact	6.56	13.02	14.63

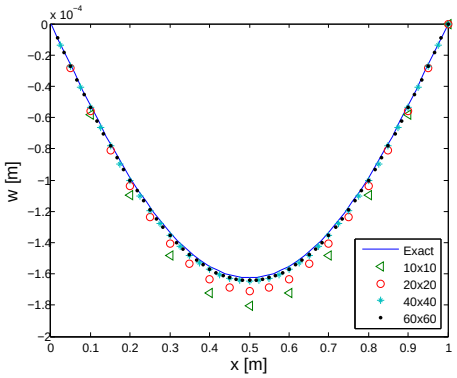

Fig. 4: The NOM results to solve the nonhomogeneous biharmonic equation [141].

nates as:

$$\nabla^4 w = \sum_{i=1}^{n}\sum_{j=1}^{n} \partial_i\partial_i\partial_j\partial_j w = \left(\sum_{i=1}^{n}\partial_i\partial_i\right)\left(\sum_{j=1}^{n}\partial_j\partial_j\right) w \qquad (34)$$

With the aid of nonlocal Hessian operator $\tilde{\nabla}^2 w$ and its variation $\tilde{\nabla}^2\delta w$, Ren et al. [141] used the NOM to solve the nonhomogeneous biharmonic equation for a simply supported square plate subjected to uniform loading as shown in Fig. 5, which shows the accuracy of NOM.

3.3. Schrödinger equation

The Schrödinger equation [176]-[180] is a linear partial differential equation that regulates a quantum-mechanical system's wave function. The Schrödinger equation for a one-dimensional

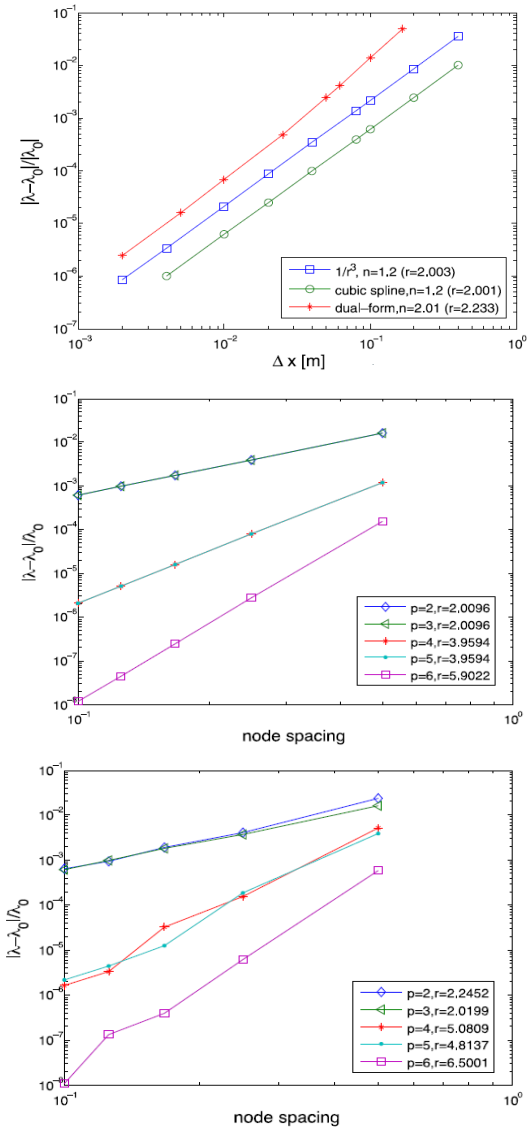

Fig. 5: Convergence of the lowest eigenvalue for a one-dimensional harmonic oscillator: (a) First-order NOM with an inhomogeneous discretization [141]; (b) Higher-order NOM with a regular node distribution [142]; (c) Higher-order NOM with a irregular node distribution [142].

harmonic oscillator is given by

$$\left[-\frac{\hbar^2}{2m}\frac{\partial^2}{\partial x^2} + V(x)\right]\phi(x,t) = i\hbar\frac{\partial}{\partial t}\phi(x,t), \quad V(x) = \frac{1}{2}\omega^2 x^2 \qquad (35)$$

where $\phi(x,t)$ denotes a wave function. The parameter m indicates the particle's mass, and

$V(x)$ denotes the potential that reflects the particle's surroundings. By using NOM, Ren et al. [141] tested the accuracy of the eigenvalue problem based on the first-order nonlocal operators; the convergence plot of the error is shown in Fig. 5.

3.4. Poisson equation

Poisson's equation [181]-[184] is an elliptic partial differential equation with widespread use in theoretical physics. The solution to Poisson's equation, for instance, is the potential field created by a particular electric charge or mass density distribution; once the potential field is known, the electrostatic or gravitational (force) field may be calculated. Poisson's equation is given by

$$\Delta \rho_* = f \tag{36}$$

where f and ρ_* represent real or complex-valued functions on a manifold. Typically, f is provided and ρ_* is requested. When the manifold is in Euclidean space, the Laplace operator is typically represented as ∇^2, and Poisson's equation is commonly written as

$$\nabla^2 \rho_* = f \tag{37}$$

It has the following form in 3D Cartesian coordinates:

$$\left(\frac{\partial^2}{\partial x^2} + \frac{\partial^2}{\partial y^2} + \frac{\partial^2}{\partial z^2} \right) \rho_*(x, y, z) = f(x, y, z) \tag{38}$$

Numerical results of the Poisson equation by the NOM are found in Fig. 6 [141]. Ren et al. [142] also solved the Poisson equation with dimensional number $n = (2, 3, 4, 5)$ under various discretization and order of nonlocal operator, with the statistical findings provided in Tab. 3.

3.5. Föppl–von Kármá equations

The Föppl-von Kármá equations [185, 186] are a set of nonlinear partial differential equations

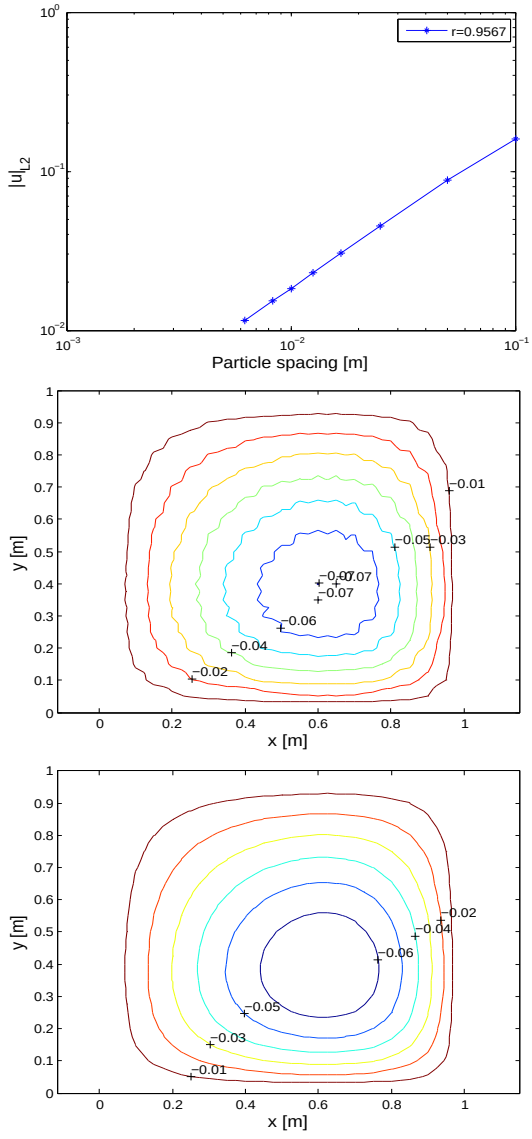

Fig. 6: (a) Convergence of the displacement's L2 error; (b) Contour of u without hourglass control for discretization 40×40; (c) Contour of u with hourglass control $\mu = 0.1$ for discretization 40×40 [141].

that describe the – large – deflections of thin plates [187]. They are given by [188]:

$$\frac{Eh^3}{12\,(1-\nu^2)} \nabla^4 w - h \frac{\partial}{\partial x_\beta} \left(\sigma_{\alpha\beta} \frac{\partial w}{\partial x_\alpha} \right) = P \tag{39}$$

$$\frac{\partial \sigma_{\alpha\beta}}{\partial x_\beta} = 0 \tag{40}$$

Tab. 3: The NOM results for different dimensional Poisson equations [142]

Dimension	Nnode	Δx	L_2 norm	$\frac{u_{max}}{u_{max}^{exact}} - 1$	p-order	p^{hg}
2 dimension	1681	0.025	0.0485	-0.0281	1	1
	1681	0.025	0.0262	0.01	2	1
	1681	0.025	0.0139	-0.00256	3	1
	1681	0.025	0.0175	-0.00308	4	1
	6561	0.0125	0.0379	0.033	1	0
	6561	0.0125	0.0179	0.0714	1	1
	6561	0.0125	0.011	0.00505	2	1
	25921	0.00625	0.0202	0.0221	1	1
	25921	0.00625	0.00501	0.00266	2	1
	25921	0.00625	0.00191	-0.000417	3	1
	40401	0.005	0.00777	-0.00263	1	1
	160801	0.0025	0.00291	0.0007	1	1
3 dimension	10648	0.04763	0.0907	-0.0406	1	1
	29791	0.03333	0.0604	-0.0248	1	1
	68921	0.025	0.0485	-0.02	1	1
4 dimension	14641	0.1	0.169	-0.0514	1	1
	65536	0.0667	0.118	-0.0171	1	1
	160000	0.0526	0.0983	-0.0203	1	1
	810000	0.0345	0.0579	0.00304	1	1
	2560000	0.0256	0.0454	0.00152	1	1
5 dimension	7776	0.2	0.229	-0.114	1	1
	100000	0.111	0.181	-0.0944	1	1
	1048576	0.0667	0.13	-0.0485	1	1
	4084101	0.05	0.0985	-0.0352	1	1

where h denotes the plate thickness, w the out-of-plane deflection of the plate, P the external normal force, σ the Cauchy stress tensor and α, β are indices (the two orthogonal in-plane directions). The biharmonic operator in 2D is defined as

$$\nabla^4 w := \frac{\partial^2}{\partial x_\alpha \partial x_\alpha}\left[\frac{\partial^2 w}{\partial x_\beta \partial x_\beta}\right] = \frac{\partial^4 w}{\partial x_1^4} + \frac{\partial^4 w}{\partial x_2^4} + 2\frac{\partial^4 w}{\partial x_1^2 \partial x_2^2} \tag{41}$$

Figure 7 illustrates the NOM solution with a ABAQUS solution based on S4R plate elements [142, 189].

3.6. Cahn-Hilliard equation

The Cahn-Hilliard equation [190]-[194] describes the process of phase separation, which occurs when two components of a binary fluid spontaneously separate and form domains in each component. If c is the fluid concentration, and $c = \pm 1$ represents domains, the equation is written as

$$\frac{\partial c}{\partial t} = D\nabla^2\left(c^3 - c - \gamma\nabla^2 c\right) \tag{42}$$

where D is the diffusion coefficient and $\sqrt{\gamma}$ is the length of the transition areas between the domains. The partial time derivative is $\partial/\partial t$, while the Laplacian in n dimensions is ∇^2. Furthermore, the number $\mu = c^3 - c - \gamma\nabla^2 c$ denotes the chemical potential.

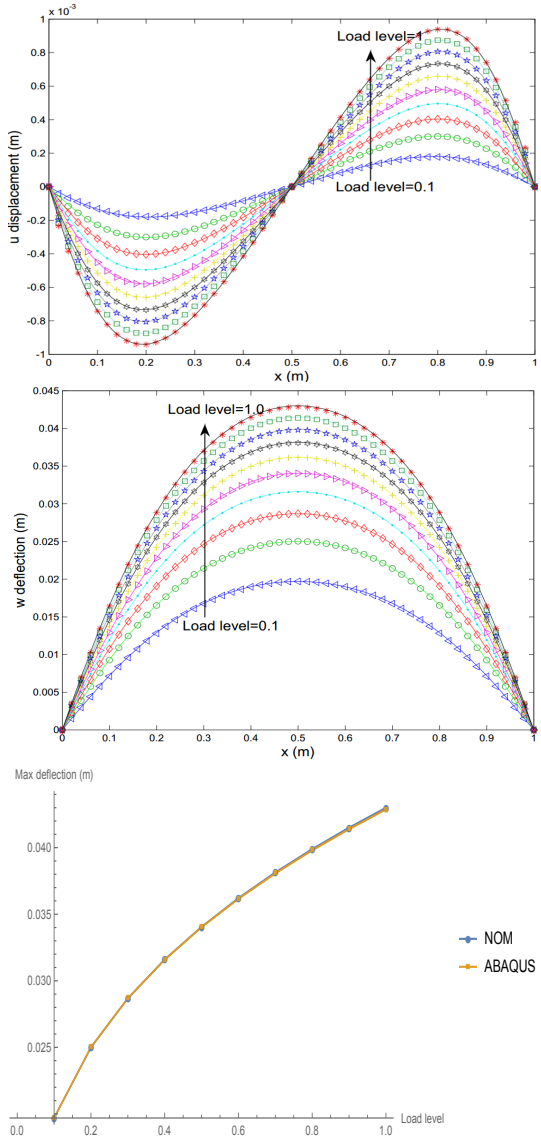

Fig. 7: Comparison between NOM results (star diamond etc symbols) and ABAQUS (lines) results: (a) Displacement for nodes in $y = L/2$; (b) Deflection for nodes in $y = L/2$; (c) Maximum deflection for middle node with a load level ranging from 0.1 to 1 [142].

Assuming period and solid-wall boundary conditions, Ren et al. [144] solved the CH equation up to 6th order using NOM exploiting NOM's higher order continuity. The results are summarized in Figs. 8-11.

3.7. Incompressible neo-Hookean model

The neo-Hookean model [195] is common used to model plastics and rubber-like material. The strain energy for the virtually incompressible Neo-Hooke material [196] can be written as

$$\mathcal{F}(\boldsymbol{F}) = \frac{1}{2}\kappa(J-1)^2 + \frac{1}{2}\mu(\boldsymbol{F}:\boldsymbol{F}-3). \quad (43)$$

where $\boldsymbol{F}$ is the deformation gradient, $J = \det \boldsymbol{F}$.

The nearly incompressible neo-Hookean model has been solved by NOM with Newton–Raphson iteration method, in [142] and agrees well with FE results, see Fig. 12 and Tab. 4.

Tab. 4: Nearly incompressible 3D model: displacement w_{max} (mm)[142]

Method/Element type	Case 1	Case 2
FEM (H1 element)	13.17 (8^3 mesh)	19.52 (32^3 mesh)
FEM (H2 element)	19.54 (8^3 mesh)	20.01 (32^3 mesh)
NOM (node)	19.14 (11^3 nodes)	20.43 (21^3 nodes)

3.8. Gradient elasticity solid problem

Gradient elasticity theory can be traced back to the Cosserat theory [198]. The Cosserat theory is based on higher-order gradients. Numerous gradient elasticity theories were developed including micro-polar solid [198], couple stress theory [199]-[201], Mindlin solid theory [202, 203], nonlocal elasticity [204] and second-grade materials [205]. To address gradient elasticity problems, a variety of theoretical solutions [206]-[210] and numerical methods [211]-[223] have been developed. The isotropic elasticity gradient material's energy functional [207, 210] can be represented as

$$\mathbb{W} = \int_\Omega \frac{1}{2}\bar{\boldsymbol{\sigma}} : \boldsymbol{\varepsilon} + \frac{\ell^2}{2}\nabla\bar{\boldsymbol{\sigma}}{:}\nabla\boldsymbol{\varepsilon}\,\mathrm{d}\Omega - \int_\Omega \boldsymbol{b}\cdot\boldsymbol{u}\mathrm{d}\Omega - \int_{\partial\Omega}\mathbb{P}\cdot\boldsymbol{u}\mathrm{d}S - \int_{\partial\Omega}\mathbb{R}\cdot(\boldsymbol{n}^*\cdot\nabla\boldsymbol{u})\mathrm{d}S \quad (44)$$

where $\bar{\boldsymbol{\sigma}}$ refers to the Cauchy-like stress tensor, l is the gradient material factor, $\boldsymbol{\varepsilon}$ =

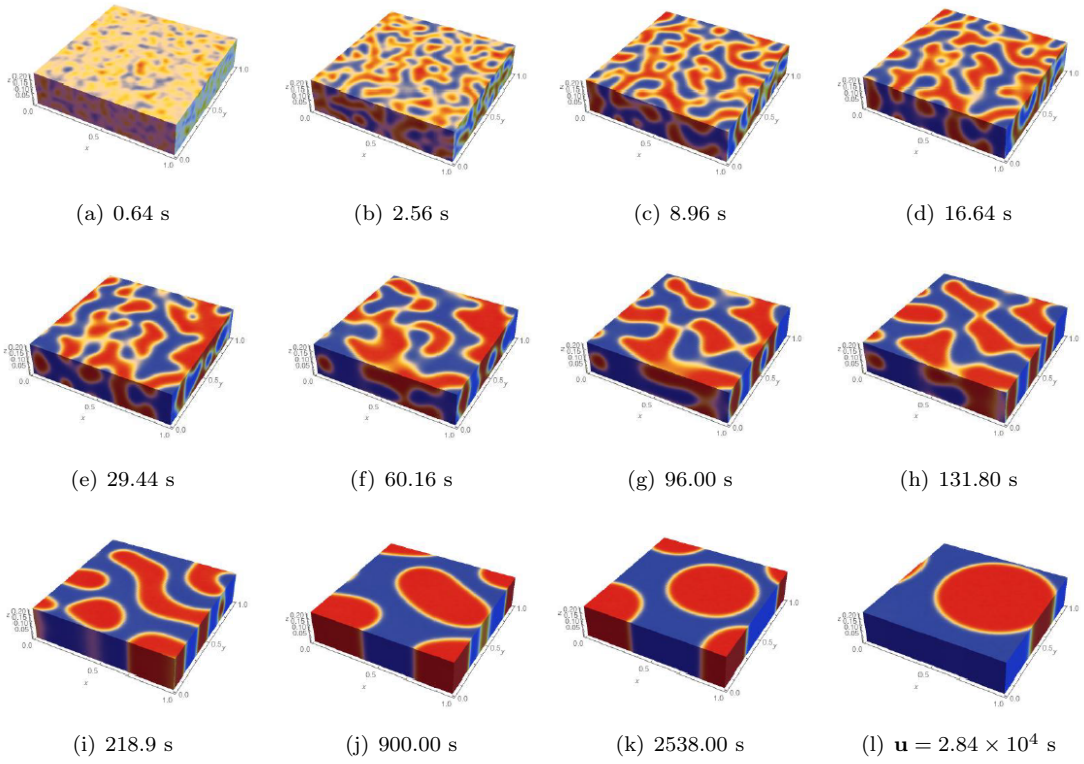

(a) 0.64 s (b) 2.56 s (c) 8.96 s (d) 16.64 s

(e) 29.44 s (f) 60.16 s (g) 96.00 s (h) 131.80 s

(i) 218.9 s (j) 900.00 s (k) 2538.00 s (l) $\mathbf{u} = 2.84 \times 10^4$ s

Fig. 8: The evolution of the Cahn-Hilliard phase field model in 3D block using NOM [144].

$\frac{1}{2}(\nabla \boldsymbol{u} + \boldsymbol{u}\nabla)$, whereas $\mathbb{P}$ and $\mathbb{R}$ represents the traction force and double traction force acting on $\partial\Omega$.

The lower gradient elasticity problem based on either the Lagrange multipliers or modified variational principle to enforce the boundary conditions has been solved by the NOM in [143], see Fig. 13. Ren et al. [145] derived the governing equations for the higher-order gradient solid, and developed a NOM and applied it finally to the higher-order gradient solid examples. The numerical tests are consistent with the numerical analysis by FEM [224] and IGA [221], which demonstrate the capability of the NOM in solving higher-order gradient elasticity problems as shown in Fig. 14 and Fig. 15.

3.9. Phase field fracture modeling

Phase-field models for fracture as presented in [225]-[229] introduce an additional field to describe the damage status of a material point. The evolution of the damage is obtained by solving an additional differential equation. Miehe et al. [225] define the fracture surface density per unit volume of the solid as

$$\Lambda(\phi, \nabla\phi) = \frac{\phi^2}{2l_0} + \frac{l_0}{2}\nabla\phi \cdot \nabla\phi \qquad (45)$$

where the phase field $\phi = 1$ denotes a totally cracked/damaged material, while $\phi = 0$ represents the intact material; l_0 is a parameter. The phase field energy functional, according to Bour-

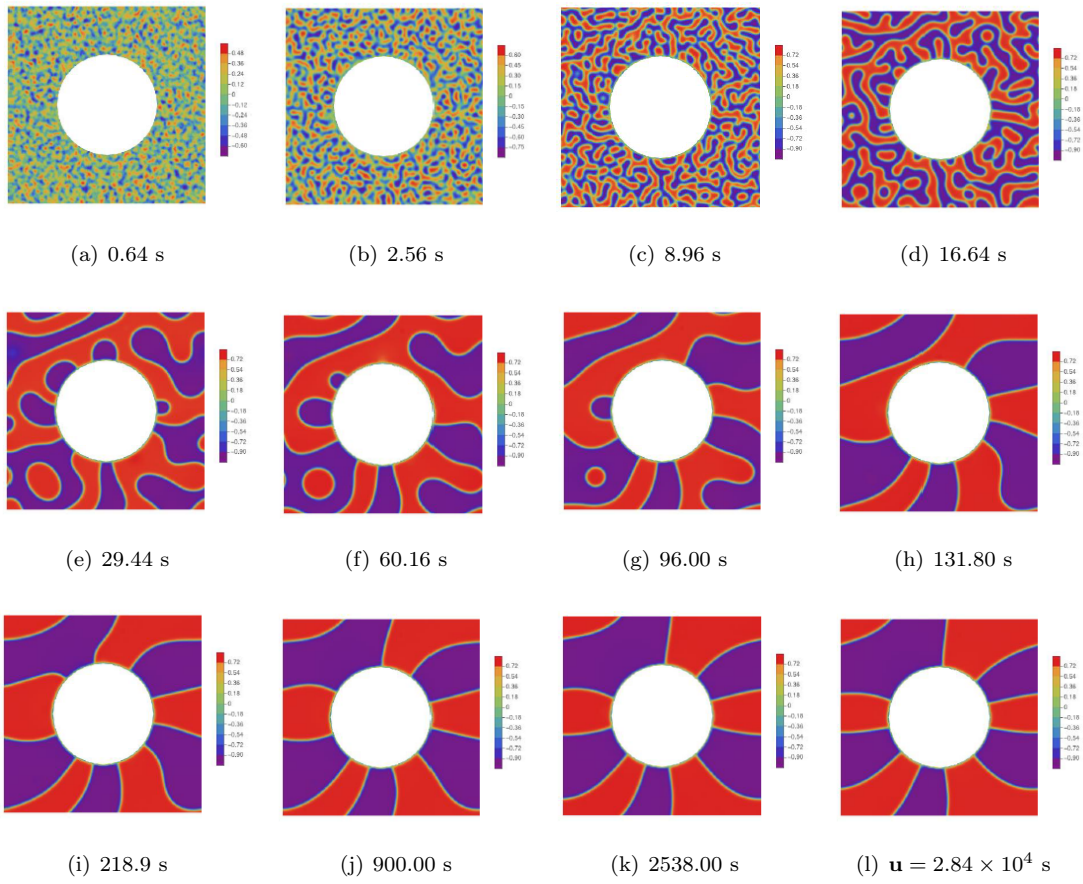

(a) 0.64 s (b) 2.56 s (c) 8.96 s (d) 16.64 s

(e) 29.44 s (f) 60.16 s (g) 96.00 s (h) 131.80 s

(i) 218.9 s (j) 900.00 s (k) 2538.00 s (l) $\mathbf{u} = 2.84 \times 10^4$ s

Fig. 9: The evolution of the Cahn-Hilliard phase field model for domain with round internal BCs using NOM [144].

din and Miehe [230, 226], can be written as

$$\begin{aligned}\Pi(\boldsymbol{u}, \phi, \Lambda) = &\int_{\Omega} G_c \Lambda(\phi, \nabla\phi) \mathrm{d}\Omega \\ &+ \int_{\Omega} \psi_{\mathbb{e}}(\boldsymbol{\varepsilon}(\mathbf{u}), \phi) \mathrm{d}\Omega \\ &- \int_{\Omega} \mathbf{b} \cdot \boldsymbol{u} \mathrm{d}\Omega - \int_{\partial\Omega_f} \boldsymbol{f} \cdot \boldsymbol{u} \mathrm{d}S \end{aligned} \quad (46)$$

where G_c denotes the critical energy release rate $\Lambda(\phi)$ and l_0 is a length scale parameter. The displacement field and elastic energy density are indicated by $\mathbf{u}$ and $\psi_{\mathbb{e}}$, respectively; the phase field $\phi(\boldsymbol{x}, t) \in [0, 1]$, smears the crack surface over a specific domain. The elastic energy is decomposed into tensile and compressive components to ensure that fracture occurs exclusively under tension [230]. The strain tensor $\boldsymbol{\varepsilon}$ can be split using the eigen-decomposition as follows:

$$\begin{aligned}\boldsymbol{\varepsilon}_+ &= \sum_{\mathbb{a}=1}^{\mathbb{b}} \langle \varepsilon_{\mathbb{a}} \rangle_+ \mathbf{n}_{\mathbb{a}} \otimes \mathbf{n}_{\mathbb{a}}, \\ \boldsymbol{\varepsilon}_- &= \sum_{\mathbb{a}=1}^{\mathbb{b}} \langle \varepsilon_{\mathbb{a}} \rangle_- \mathbf{n}_{\mathbb{a}} \otimes \mathbf{n}_{\mathbb{a}} \end{aligned} \quad (47)$$

where $\boldsymbol{\varepsilon}_+$ and $\boldsymbol{\varepsilon}_-$ are the tensile and compressive components of the strain tensor, respectively. The principal strain is $\varepsilon_{\mathbb{a}}$ and its direction $\mathbf{n}_{\mathbb{a}}$. ψ_e is separated into two parts to distinguish between the material's tensile and compressive strengths: the tensile component affected by the phase field and the compressive component that is independent of the phase field.

$$\begin{aligned}\psi_e(\boldsymbol{\varepsilon}(\nabla \boldsymbol{u}), \phi) = &[(1-\phi)^2 + \kappa_0] \psi_e^+(\boldsymbol{\varepsilon}(\nabla \boldsymbol{u})) \\ &+ \psi_e^-(\boldsymbol{\varepsilon}(\nabla \boldsymbol{u})) \end{aligned} \quad (48)$$

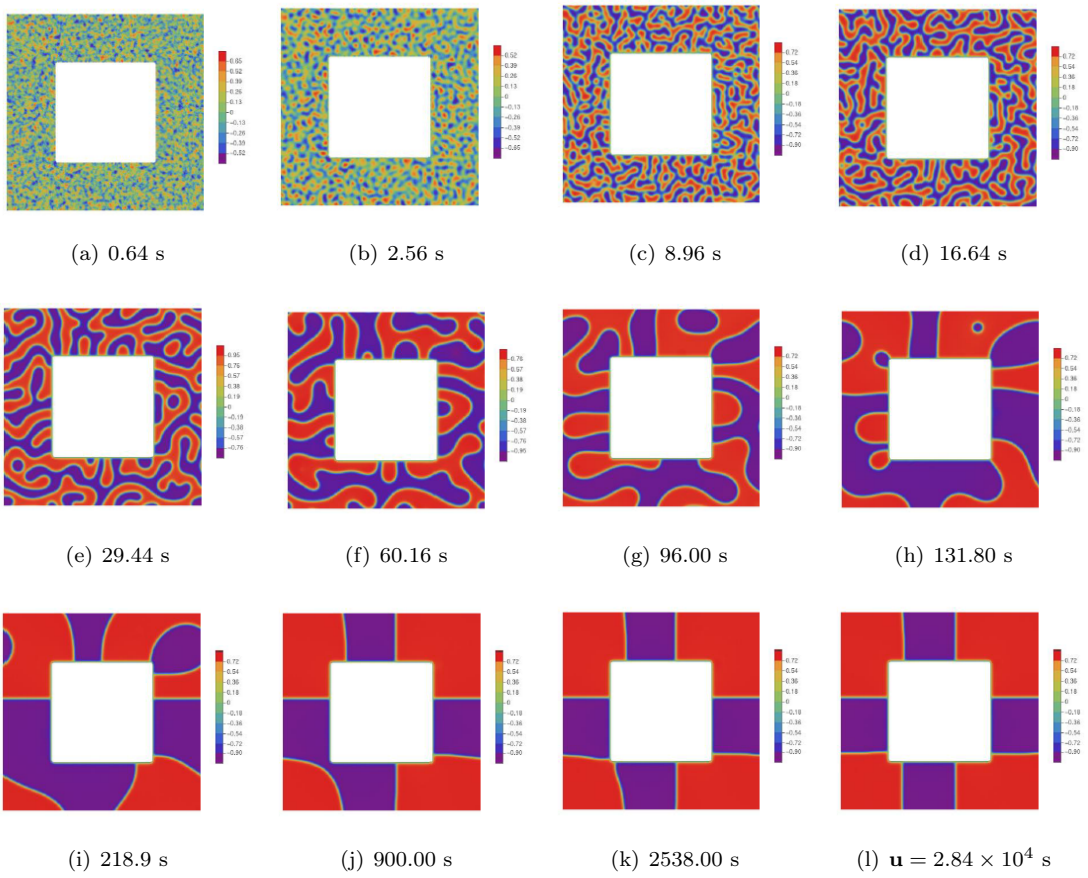

(a) 0.64 s (b) 2.56 s (c) 8.96 s (d) 16.64 s

(e) 29.44 s (f) 60.16 s (g) 96.00 s (h) 131.80 s

(i) 218.9 s (j) 900.00 s (k) 2538.00 s (l) $\mathbf{u} = 2.84 \times 10^4$ s

Fig. 10: The evolution of the Cahn-Hilliard phase field model for domain with square internal BCs using NOM [144].

where κ_0 ($\kappa_0 > 0$ and $\kappa_0 \ll 1$) denotes a small positive factor. The phase field governing equations are written as

$$\begin{cases} \nabla \cdot \boldsymbol{\sigma} + \mathbf{b} = 0 \\ G_c \left(\phi - l^2 \nabla^2 \phi\right) = 2l(1-\phi)H \end{cases} \tag{49}$$

where $H(\mathbf{x}, T) := \max_{t \in [0,T]} \psi_e^+(\boldsymbol{\varepsilon}(\mathbf{x}, t))$ [226]; $\boldsymbol{\sigma}$ is the Cauchy stress. The phase field model has been implemented using FEMs or IGA [231, 226, 232, 233, 234, 23] and in NOM in [147, 148], see Fig. 16 and Fig. 17.

4. Future perspectives of NOM

Although NOM has been successfully used to solve various PDEs, the majority of the issues that have been addressed are limited to continuous problems as summarized in Tab. 5. Other potential NOM applications still remain unexplored and can be found in Tab. 6. They could exploit the higher-order continuity of NOM and its ease in implementation. Since NOM can be considered as an extension of PD, it can also exploits PD's ability to naturally deal with discrete material failure and fracture.

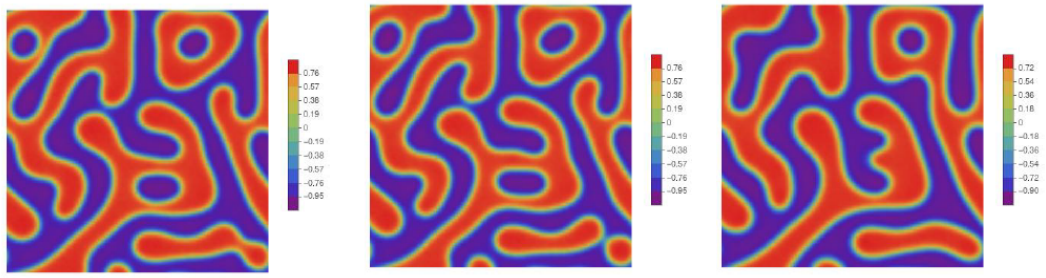

(a) $\ell = 0$, $t = 24$ s (b) $\ell = 0.1\Delta x$, $t = 20$ s (c) $\ell = 0.5\Delta x$, $t = 30$ s

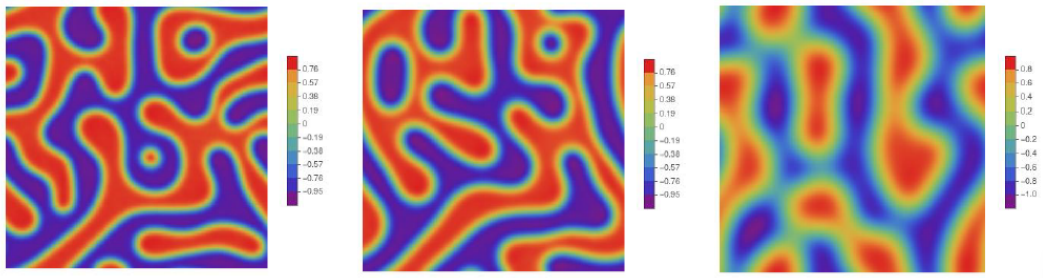

(d) $\ell = \Delta x$, $t = 24$ s (e) $\ell = 2\Delta x$, $t = 30$ s (f) $\ell = 10\Delta x$, $t = 18$ s

Fig. 11: The early-stage 6th-order CH equation phase field model vs ℓ [144].

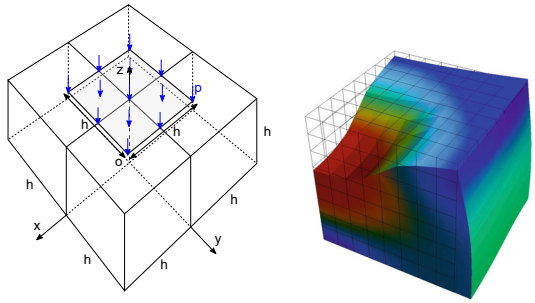

(a) Setup of the model. (b) FEM with 8^3 mesh [197]

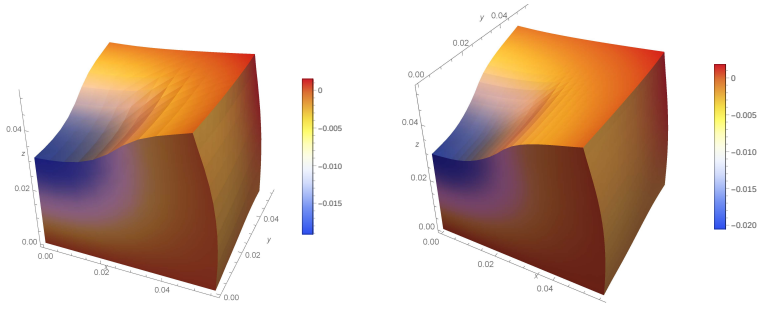

(c) NOM with 11^3 nodes (d) NOM with 21^3 nodes

Fig. 12: (a) Setup of the model; (b)-(d) z-direction displacement in deformed configuration [142].

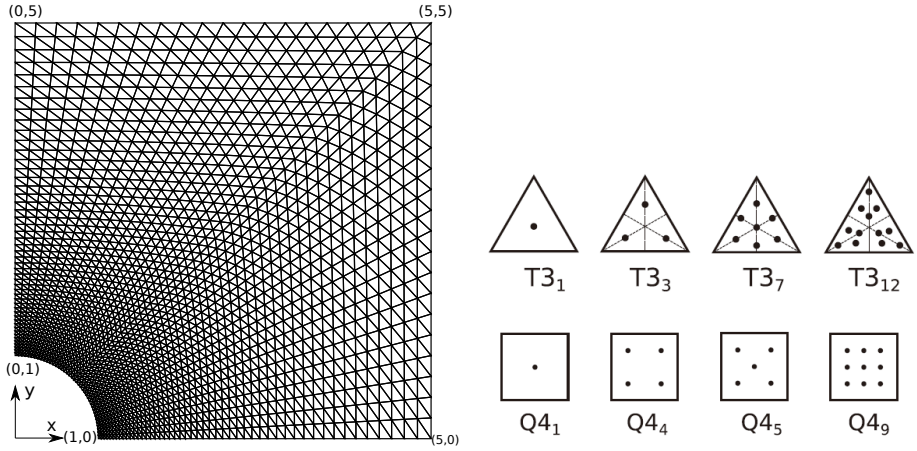

(a) (b)

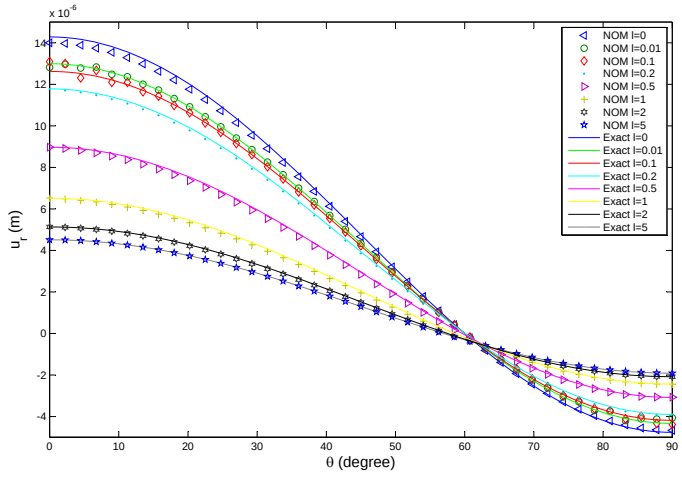

(c)

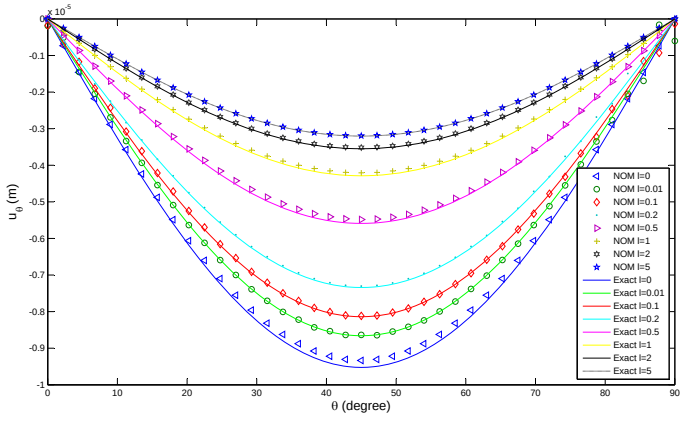

(d)

Fig. 13: (a) setup and mesh of the plate; (b) numerical integration scheme; (c-d) u_r and u_θ on $r = a$ for various gradient coefficient l [143].

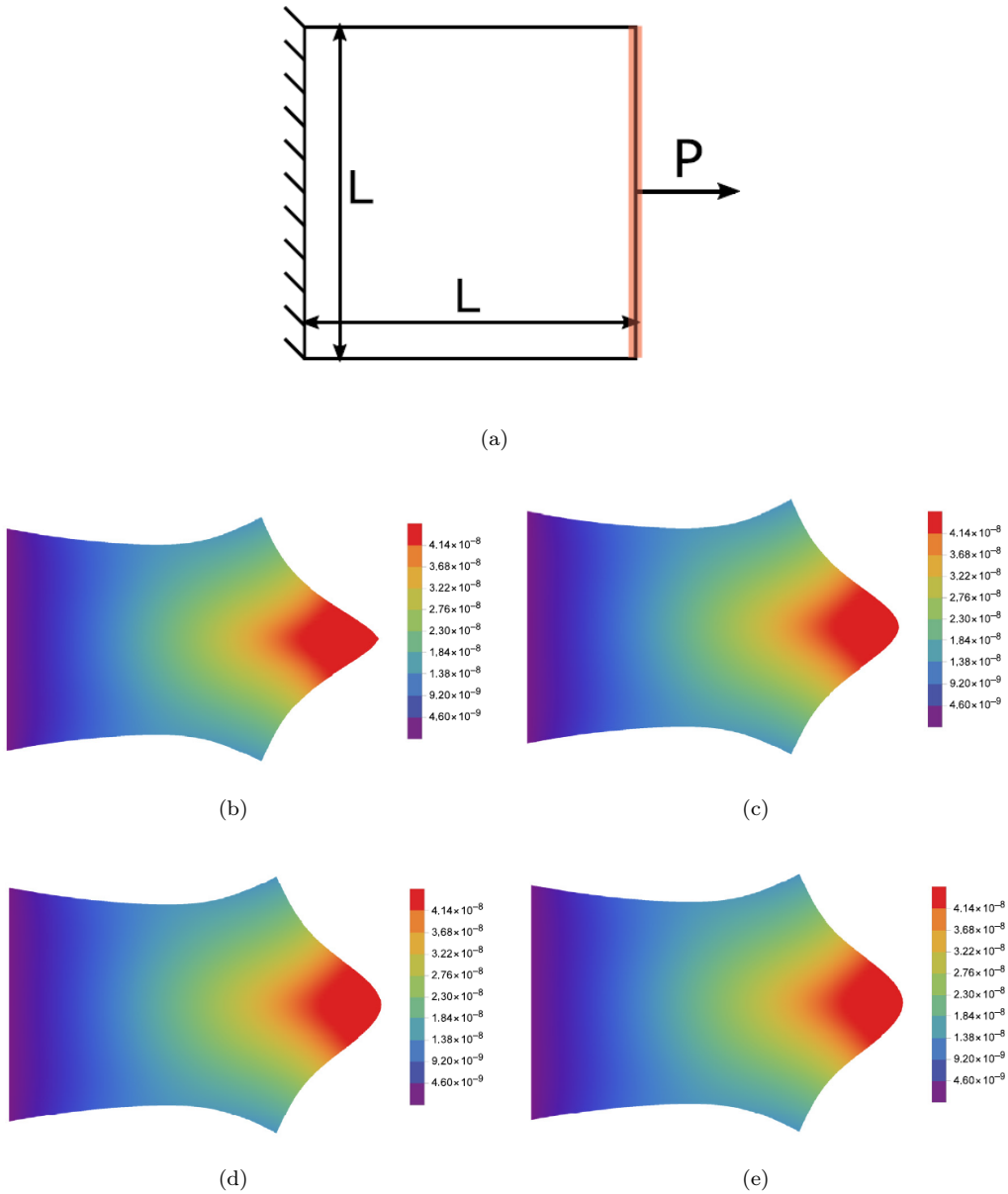

(a)

(b)

(c)

(d)

(e)

Fig. 14: (a) Setup of the plate; (b)-(e) Displacement in x-direction with deformation for E^1, E^2, E^3 and E^4 elasticity [145].

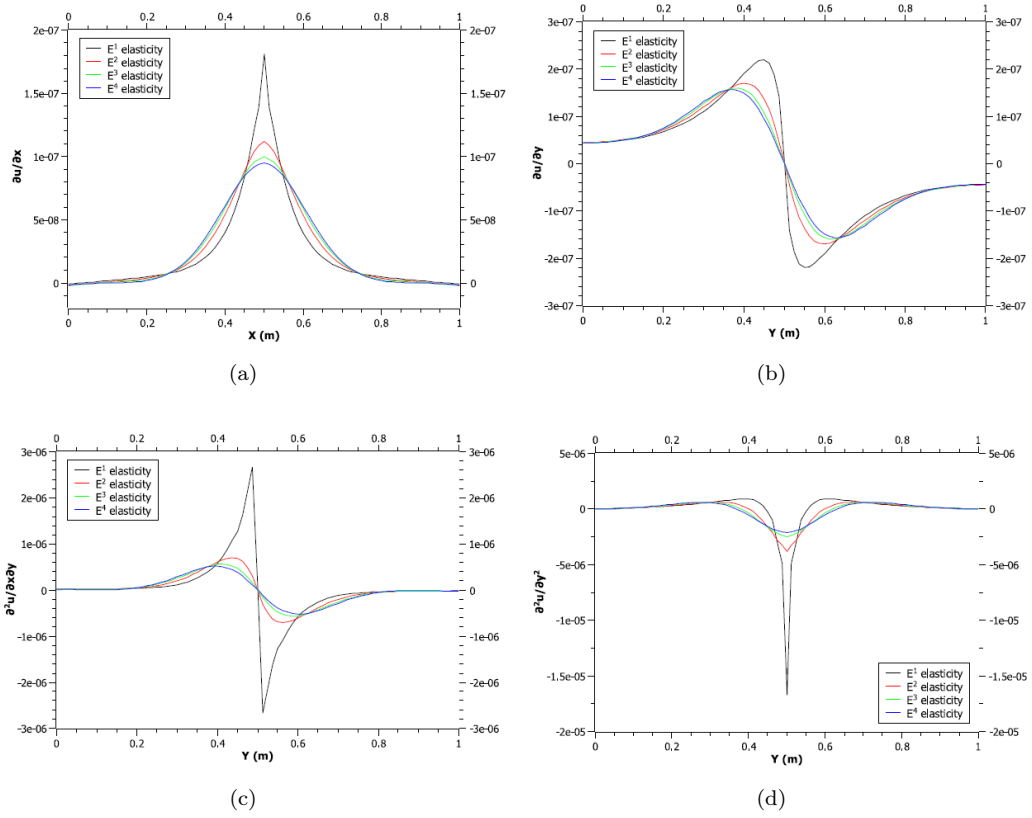

Fig. 15: (a)-(d)The derivative of deformation of all points on the right line for $\frac{\partial u}{\partial x}$, $\frac{\partial u}{\partial y}$, $\frac{\partial^2 u}{\partial x \partial y}$ and $\frac{\partial^2 u}{\partial y^2}$ [145].

Tab. 5: Successful NOM applications

Successful NOM applications
• Electromagnetic waveguide problems [140]
• 1D Schrödinger equation [141, 142]
• Poisson equation [141, 142]
• Von Kármán equations for a thin plate [142]
• Nonhomogeneous biharmonic equation [142]
• Nearly incompressible block [142]
• Gradient elasticity problems [143]
• Cahn-Hilliard phase field model[144]
• Finite deformation higher-order gradient elasticity [145]
• Quasi-static and dynamic fracture modeling [147, 148]

5. Conclusions

In this paper, we reviewed developments of the NOM, a novel approach to solve PDEs and challenging problems in engineering. Three NOM versions have been proposed so far: first-order/higher-order particle-based NOM and higher-order 'numerical integration-based' NOM. The first version NOM is based on common nonlocal operators. These nonlocal operators employ the first-order of the TSE. The operator energy functional is introduced

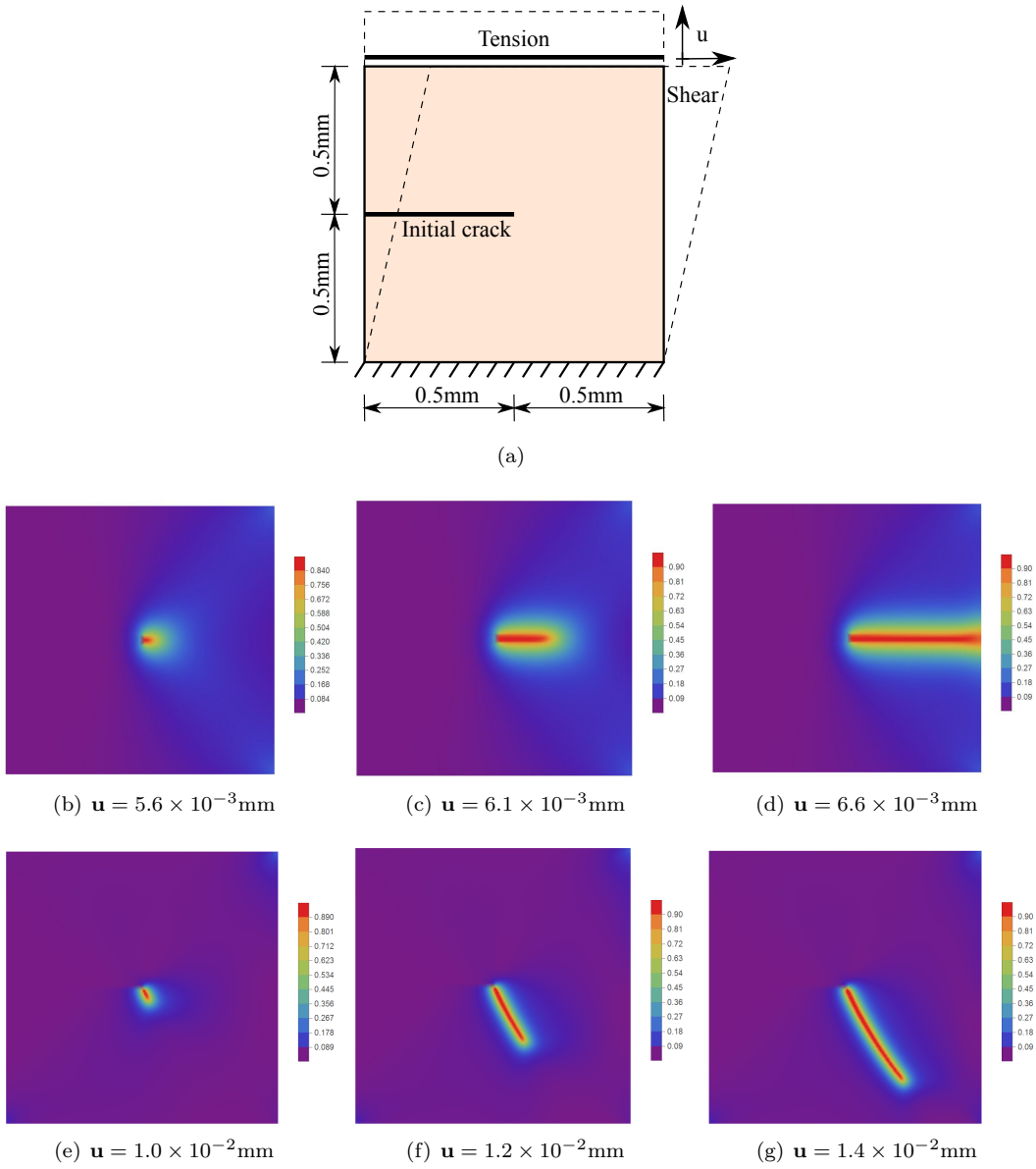

(a)

(b) $\mathbf{u} = 5.6 \times 10^{-3}$mm (c) $\mathbf{u} = 6.1 \times 10^{-3}$mm (d) $\mathbf{u} = 6.6 \times 10^{-3}$mm

(e) $\mathbf{u} = 1.0 \times 10^{-2}$mm (f) $\mathbf{u} = 1.2 \times 10^{-2}$mm (g) $\mathbf{u} = 1.4 \times 10^{-2}$mm

Fig. 16: (a) Geometry and boundary conditions; phase field (b-d) evolution process for $l_0 = 0.0375$ mm in tension test; phase field (e-g) evolution process for $l_0 = 0.015$ mm in shear test [147].

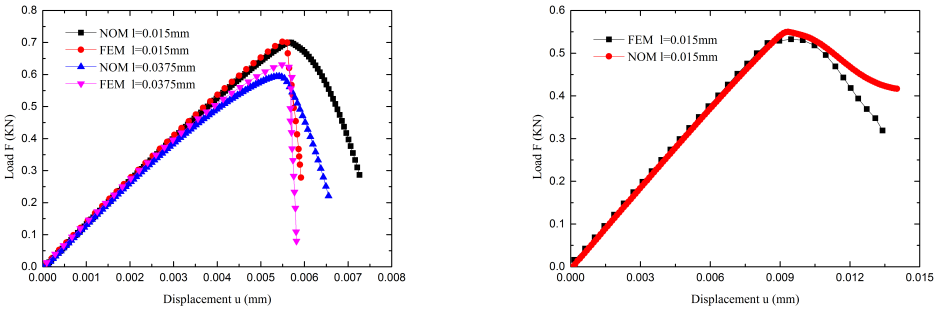

(a) (b)

Fig. 17: Reaction force-displacement curves in tension (a)/shear (b) test [147].

Tab. 6: Future NOM applications

Future NOM applications
• Material nonlinearities including plasticity, viscoelasticity and viscoplasticity.
• Multi-physics problems (coupled thermo-mechanical, electro-mechanical, electro-chemical problems to name a few) exploiting the ease in implementation.
• Plate and shell problems, especially higher-order theories or theories of thin plate/shell analysis exploiting the higher-order continuity of NOM. When NOM is applied to a curvilinear coordinate system, it is also viable to handle shell problems.
• Higher order gradient (elastoplasticity) problems exploiting the higher-order continuity of NOM
• Finite strain and/or large deformation problems exploiting the 'meshfree character' of NOM.
• The wave propagation analysis of gradient elasticity problems and studying – in this context – interesting phenomena like size, surface and nonlocal effects.
• Modeling of discontinuities as they occur in fracture/crack propagation in solids, fluid-structure interaction or fluid mechanics such as two-phase flow.
• Higher-order PDEs on stationary and evolving surface exploiting the higher-order continuity of NOM including its ease in implementation.

to eliminate the zero-energy model. The first version of NOM is appropriate for C^0 continuity problems such as solid mechanics and phase-field fracture models. The second version of NOM generalizes the first version of NOM by employing a higher-order TSE. Higher-order TSE can provide arbitrary order partial derivatives in any dimension. These higher-order derivatives are appropriate for higher-order PDEs as required in some plate theories or strain gradient solid mechanics. Higher-order NOM considerably improves NOM's capacity to solve more complex issues. The third version of NOM employs accurate numerical integration. The boundary conditions of various orders can be accurately applied as combined with the Lagrange multiplier or modified variational principle. NOM has been successfully applied to the solutions of various lower-order and higher-order PDEs. The nonlocal operators for a given energy function can be constructed automatically using the highest order of partial derivative and spacial dimensions, and NOM can also be utilized to derive the nonlocal strong form based on variational principles. The NOM obtains the residual and tangent stiffness matrix simply and efficiently. In the near future, the power of NOM in deriving nonlocal models remains largely unexplored. NOM will be applied to the solutions for many

complicated physical PDEs problems, such as gradient plate problems, higher order gradient (elastoplasticity) problems, higher-order PDEs on the stationary and evolving surfaces to name only a few.

Acknowledgments

The financial support provided by China Scholarship Council is gratefully acknowledged.

References

[1] Zienkiewicz, O.C., Taylor, R.L., Zienkiewicz, O.C., & Taylor, R.L. (1977). *The finite element method*, volume 36. McGraw-hill London.

[2] Larsson, S. & Thomée, V. (2003). *Partial differential equations with numerical methods*, volume 45. Springer.

[3] Ŝolín, P. (2005). *Partial differential equations and the finite element method*, volume 73. John Wiley & Sons.

[4] Jiang, Y. & Ma, J. (2011). High-order finite element methods for time-fractional partial differential equations. *Journal of Computational and Applied Mathematics*, *235*(11), 3285–3290.

[5] Grande, J. & Reusken, A. (2016). A higher order finite element method for partial differential equations on surfaces. *SIAM Journal on Numerical Analysis*, *54*(1), 388–414.

[6] Feng, X., Hennings, L., & Neilan, M. (2017). Finite element methods for second order linear elliptic partial differential equations in non-divergence form. *Mathematics of Computation*, *86*(307), 2025–2051.

[7] Hossain, M.N., Paladim, D., Vogel, F., & Bordas, S. (2013). Implementation of a XFEM toolbox in Diffpack. In *International Conference on Extended Finite Element Methods-XFEM 2013, September 11–13, 2013, Lyon, France*.

[8] Wang, T., Yang, C., & Xie, X. (2018). Nitsche-XFEM for optimal control problems governed by elliptic PDEs with interfaces. *arXiv preprint arXiv:180503944*.

[9] Liu, W.K., Jun, S., & Zhang, Y.F. (1995). Reproducing kernel particle methods. *International journal for numerical methods in fluids*, *20*(8-9), 1081–1106.

[10] Huang, T.H., Wei, H., Chen, J.S., & Hillman, M.C. (2020). RKPM2D: an open-source implementation of nodally integrated reproducing kernel particle method for solving partial differential equations. *Computational particle mechanics*, *7*(2), 393–433.

[11] Chen, J.S., Liu, W.K., Hillman, M.C., Chi, S.W., Lian, Y., & Bessa, M.A. (2017). Reproducing kernel particle method for solving partial differential equations. *Encyclopedia of Computational Mechanics Second Edition*, 1–44.

[12] Jia, Y., Zhang, Y., Xu, G., Zhuang, X., & Rabczuk, T. (2013). Reproducing kernel triangular B-spline-based FEM for solving PDEs. *Computer Methods in Applied Mechanics and Engineering*, *267*, 342–358.

[13] Nayroles, B., Touzot, G., & Villon, P. (1992). Generalizing the finite element method: diffuse approximation and diffuse elements. *Computational mechanics*, *10*(5), 307–318.

[14] Krongauz, Y. & Belytschko, T. (1997). A Petrov-Galerkin diffuse element method (PG DEM) and its comparison to EFG. *Computational Mechanics*, *19*(4), 327–333.

[15] Babuška, I. & Melenk, J.M. (1997). The partition of unity method. *International journal for numerical methods in engineering*, *40*(4), 727–758.

[16] Larsson, E., Shcherbakov, V., & Heryudono, A. (2017). A least squares radial basis function partition of unity

method for solving PDEs. *SIAM Journal on Scientific Computing*, *39*(6), A2538–A2563.

[17] Griebel, M. & Schweitzer, M.A. (2000). A particle-partition of unity method for the solution of elliptic, parabolic, and hyperbolic PDEs. *SIAM Journal on Scientific Computing*, *22*(3), 853–890.

[18] Safdari-Vaighani, A., Heryudono, A., & Larsson, E. (2015). A radial basis function partition of unity collocation method for convection–diffusion equations arising in financial applications. *Journal of Scientific Computing*, *64*(2), 341–367.

[19] De Falco, C., Reali, A., & Vázquez, R. (2011). GeoPDEs: a research tool for isogeometric analysis of PDEs. *Advances in Engineering Software*, *42*(12), 1020–1034.

[20] Tagliabue, A., Dede, L., & Quarteroni, A. (2014). Isogeometric analysis and error estimates for high order partial differential equations in fluid dynamics. *Computers & Fluids*, *102*, 277–303.

[21] Bartezzaghi, A., Dedè, L., & Quarteroni, A. (2015). Isogeometric analysis of high order partial differential equations on surfaces. *Computer Methods in Applied Mechanics and Engineering*, *295*, 446–469.

[22] Dalcin, L., Collier, N., Vignal, P., Côrtes, A., & Calo, V.M. (2016). PetIGA: A framework for high-performance isogeometric analysis. *Computer Methods in Applied Mechanics and Engineering*, *308*, 151–181.

[23] Valizadeh, N. & Rabczuk, T. (2019). Isogeometric analysis for phase-field models of geometric PDEs and high-order PDEs on stationary and evolving surfaces. *Computer Methods in Applied Mechanics and Engineering*, *351*, 599–642.

[24] Langer, U. & Moore, S.E. (2016). Discontinuous Galerkin isogeometric analysis of elliptic PDEs on surfaces. In *Domain decomposition methods in science and engineering XXII*, Springer, 319–326.

[25] Garotta, F., Demo, N., Tezzele, M., Carraturo, M., Reali, A., & Rozza, G. (2020). Reduced order isogeometric analysis approach for pdes in parametrized domains. In *Quantification of Uncertainty: Improving Efficiency and Technology*, Springer, 153–170.

[26] Aluru, N. (2000). A point collocation method based on reproducing kernel approximations. *International Journal for Numerical Methods in Engineering*, *47*(6), 1083–1121.

[27] Hu, H.Y., Chen, J.S., & Hu, W. (2011). Error analysis of collocation method based on reproducing kernel approximation. *Numerical Methods for Partial Differential Equations*, *27*(3), 554–580.

[28] Cialenco, I., Fasshauer, G.E., & Ye, Q. (2012). Approximation of stochastic partial differential equations by a kernel-based collocation method. *International Journal of Computer Mathematics*, *89*(18), 2543–2561.

[29] Fasshauer, G.E. & Ye, Q. (2013). A kernel-based collocation method for elliptic partial differential equations with random coefficients. In *Monte Carlo and Quasi-Monte Carlo Methods 2012*, Springer, 331–347.

[30] Mohammadi, M. & Mokhtari, R. (2014). A reproducing kernel method for solving a class of nonlinear systems of PDEs. *Mathematical Modelling and Analysis*, *19*(2), 180–198.

[31] Mohammadi, M., Zafarghandi, F.S., Babolian, E., & Jvadi, S. (2018). A local reproducing kernel method accompanied by some different edge improvement techniques: application to the Burgers' equation. *Iranian Journal of Science and Technology, Transactions A: Science*, *42*(2), 857–871.

[32] Mahdavi, A., Chi, S.W., & Zhu, H. (2019). A gradient reproducing kernel collocation method for high order differential equations. *Computational Mechanics*, *64*(5), 1421–1454.

[33] Mahdavi, A., Chi, S.W., & Kamali, N. (2020). Harmonic-enriched reproducing kernel approximation for highly oscillatory differential equations. *Journal of Engineering Mechanics*, *146*(4), 04020014.

[34] Belytschko, T., Lu, Y.Y., & Gu, L. (1994). Element-free Galerkin methods. *International journal for numerical methods in engineering*, *37*(2), 229–256.

[35] Deb, M.K., Babuška, I.M., & Oden, J.T. (2001). Solution of stochastic partial differential equations using Galerkin finite element techniques. *Computer Methods in Applied Mechanics and Engineering*, *190*(48), 6359–6372.

[36] Babuska, I., Tempone, R., & Zouraris, G.E. (2004). Galerkin finite element approximations of stochastic elliptic partial differential equations. *SIAM Journal on Numerical Analysis*, *42*(2), 800–825.

[37] Antonietti, P.F., Cangiani, A., Collis, J., Dong, Z., Georgoulis, E.H., Giani, S., & Houston, P. (2016). Review of discontinuous Galerkin finite element methods for partial differential equations on complicated domains. In *Building bridges: connections and challenges in modern approaches to numerical partial differential equations*, Springer, 281–310.

[38] Duarte, C.A. & Oden, J.T. (1996). An hp adaptive method using clouds. *Computer methods in applied mechanics and engineering*, *139*(1-4), 237–262.

[39] Liszka, T. (1984). An interpolation method for an irregular net of nodes. *International Journal for Numerical Methods in Engineering*, *20*(9), 1599–1612.

[40] Ureña, F., Salete, E., Benito, J.J., & Gavete, L. (2012). Solving third-and fourth-order partial differential equations using GFDM: application to solve problems of plates. *International Journal of Computer Mathematics*, *89*(3), 366–376.

[41] Gavete, L., Ureña, F., Benito, J.J., García, A., Ureña, M., & Salete, E. (2017). Solving second order non-linear elliptic partial differential equations using generalized finite difference method. *Journal of Computational and Applied Mathematics*, *318*, 378–387.

[42] Ureña, F., Gavete, L., Garcia, A., Benito, J.J., & Vargas, A.M. (2019). Solving second order non-linear parabolic PDEs using generalized finite difference method (GFDM). *Journal of Computational and Applied Mathematics*, *354*, 221–241.

[43] Ureña, F., Gavete, L., García, A., Benito, J.J., & Vargas, A.M. (2020). Solving second order non-linear hyperbolic PDEs using generalized finite difference method (GFDM). *Journal of Computational and Applied Mathematics*, *363*, 1–21.

[44] Lucy, L.B. (1977). A numerical approach to the testing of the fission hypothesis. *The astronomical journal*, *82*, 1013–1024.

[45] Liu, G.R. & Liu, M.B. (2003). *Smoothed particle hydrodynamics: a meshfree particle method*. World scientific.

[46] Liu, M., Liu, G., & Lam, K. (2003). Constructing smoothing functions in smoothed particle hydrodynamics with applications. *Journal of Computational and applied Mathematics*, *155*(2), 263–284.

[47] Liu, M. & Liu, G.R. (2006). Restoring particle consistency in smoothed particle hydrodynamics. *Applied numerical mathematics*, *56*(1), 19–36.

[48] Chen, J. & Beraun, J. (2000). A generalized smoothed particle hydrodynamics method for nonlinear dynamic problems. *Computer Methods in Applied Mechanics and Engineering*, *190*(1-2), 225–239.

[49] Silling, S.A., Epton, M., Weckner, O., Xu, J., & Askari, E. (2007). Peridynamic states and constitutive modeling. *Journal of Elasticity*, *88*(2), 151–184.

[50] Di Paola, M., Failla, G., & Zingales, M. (2009). Physically-based approach to the mechanics of strong non-local linear elasticity theory. *Journal of Elasticity*, *97*(2), 103–130.

[51] Di Paola, M., Failla, G., & Zingales, M. (2010). The mechanically-based approach to 3D non-local linear elasticity theory: Long-range central interactions. *International Journal of Solids and Structures*, *47*(18-19), 2347–2358.

[52] Emmrich, E. & Weckner, O. (2007). Analysis and numerical approximation of an integro-differential equation modeling non-local effects in linear elasticity. *Mathematics and mechanics of solids*, *12*(4), 363–384.

[53] Bertoldi, K., Bigoni, D., & Drugan, W. (2007). Structural interfaces in linear elasticity. Part I: Nonlocality and gradient approximations. *Journal of the Mechanics and Physics of Solids*, *55*(1), 1–34.

[54] Weckner, O., Brunk, G., Epton, M.A., Silling, S.A., & Askari, E. (2009). Green's functions in non-local three-dimensional linear elasticity. *Proceedings of the Royal Society A: Mathematical, Physical and Engineering Sciences*, *465*(2111), 3463–3487.

[55] Eringen, A.C. (1972). On nonlocal fluid mechanics. *International Journal of Engineering Science*, *10*(6), 561–575.

[56] Caffarelli, L.A. & Vasseur, A. (2012). The De Giorgi method for nonlocal fluid dynamics. In *Nonlinear partial differential equations*, Springer, 1–38.

[57] El-Nabulsi, R.A. (2018). Jerk in Planetary systems and rotational dynamics, nonlocal motion relative to earth and nonlocal fluid dynamics in rotating earth frame. *Earth, Moon, and Planets*, *122*(1), 15–41.

[58] Eringen, A.C. (1992). Vistas of nonlocal continuum physics. *International journal of engineering science*, *30*(10), 1551–1565.

[59] Eringen, A.C. (2002). *Nonlocal continuum field theories*. Springer Science & Business Media.

[60] Eringen, A.C. & Wegner, J. (2003). Nonlocal continuum field theories. *Appl Mech Rev*, *56*(2), B20–B22.

[61] Rafii-Tabar, H., Ghavanloo, E., & Fazelzadeh, S.A. (2016). Nonlocal continuum-based modeling of mechanical characteristics of nanoscopic structures. *Physics Reports*, *638*, 1–97.

[62] Eringen, A.C. (1973). Theory of nonlocal electromagnetic elastic solids. *Journal of Mathematical Physics*, *14*(6), 733–740.

[63] Mikki, S. (2020). Theory of Electromagnetic Radiation in Nonlocal Metamaterials—Part I: Foundations. *Progress In Electromagnetics Research B*, *89*, 63–86.

[64] Mikki, S. (2020). Theory of Electromagnetic Radiation in Nonlocal Metamaterials—Part II: Applications. *Progress In Electromagnetics Research B*, *89*, 87–109.

[65] Bažant, Z.P. & Jirásek, M. (2002). Nonlocal integral formulations of plasticity and damage: survey of progress. *Journal of Engineering Mechanics*, *128*(11), 1119–1149.

[66] Samal, M., Seidenfuss, M., Roos, E., Dutta, B., & Kushwaha, H. (2008). Finite element formulation of a new nonlocal damage model. *Finite Elements in Analysis and Design*, *44*(6-7), 358–371.

[67] Jirásek, M. (2007). Nonlocal damage mechanics. *Revue européenne de génie civil*, *11*(7-8), 993–1021.

[68] Borino, G., Failla, B., & Parrinello, F. (2003). A symmetric nonlocal damage theory. *International Journal of Solids and Structures*, *40*(13-14), 3621–3645.

[69] Gunzburger, M. & Lehoucq, R.B. (2010). A nonlocal vector calculus with application to nonlocal boundary value problems. *Multiscale Modeling & Simulation*, *8*(5), 1581–1598.

[70] Du, Q., Gunzburger, M., Lehoucq, R.B., & Zhou, K. (2013). A nonlocal vector calculus, nonlocal volume-constrained problems, and nonlocal balance laws. *Mathematical Models and Methods in Applied Sciences*, *23*(03), 493–540.

[71] Silling, S. (2000). Reformulation of elasticity theory for discontinuities and long-range forces. *Journal of the Mechanics and Physics of Solids*, *48*(1), 175–209.

[72] Silling, S.A. (2000). Reformulation of elasticity theory for discontinuities and long-range forces. *Journal of the Mechanics and Physics of Solids*, *48*(1), 175–209.

[73] Silling, S.A. & Askari, E. (2005). A meshfree method based on the peridynamic model of solid mechanics. *Computers & structures*, *83*(17-18), 1526–1535.

[74] Silling, S.A., Epton, M., Weckner, O., Xu, J., & Askari, E. (2007). Peridynamic states and constitutive modeling. *Journal of Elasticity*, *88*(2), 151–184.

[75] Silling, S.A. & Lehoucq, R.B. (2008). Convergence of peridynamics to classical elasticity theory. *Journal of Elasticity*, *93*(1), 13.

[76] Silling, S.A. & Lehoucq, R.B. (2010). Peridynamic theory of solid mechanics. In *Advances in applied mechanics*, volume 44, Elsevier, 73–168.

[77] Silling, S.A. & Bobaru, F. (2005). Peridynamic modeling of membranes and fibers. *International Journal of Non-Linear Mechanics*, *40*(2-3), 395–409.

[78] Silling, S.A., Weckner, O., Askari, E., & Bobaru, F. (2010). Crack nucleation in a peridynamic solid. *International Journal of Fracture*, *162*(1), 219–227.

[79] Ballarini, R., Diana, V., Biolzi, L., & Casolo, S. (2018). Bond-based peridynamic modelling of singular and nonsingular crack-tip fields. *Meccanica*, *53*(14), 3495–3515.

[80] Gu, X., Zhang, Q., & Madenci, E. (2019). Refined bond-based peridynamics for thermal diffusion. *Engineering Computations*.

[81] Wang, Y., Zhou, X., & Kou, M. (2019). An improved coupled thermo-mechanic bond-based peridynamic model for cracking behaviors in brittle solids subjected to thermal shocks. *European Journal of Mechanics-A/Solids*, *73*, 282–305.

[82] Han, D., Zhang, Y., Wang, Q., Lu, W., & Jia, B. (2019). The review of the bond-based peridynamics modeling. *Journal of Micromechanics and Molecular Physics*, *4*(01), 1830001.

[83] Yu, H., Chen, X., & Sun, Y. (2020). A generalized bond-based peridynamic model for quasi-brittle materials enriched with bond tension–rotation–shear coupling effects. *Computer Methods in Applied Mechanics and Engineering*, *372*, 113405.

[84] Amani, J., Oterkus, E., Areias, P., Zi, G., Nguyen-Thoi, T., & Rabczuk, T. (2016). A non-ordinary state-based peridynamics formulation for thermoplastic fracture. *International Journal of Impact Engineering*, *87*, 83–94.

[85] Zhou, X.P. & Wang, Y.T. (2016). Numerical simulation of crack propagation and coalescence in pre-cracked rock-like Brazilian disks using the non-ordinary state-based peridynamics. *International Journal of Rock Mechanics and Mining Sciences*, *89*, 235–249.

[86] Wang, Y., Zhou, X., & Xu, X. (2016). Numerical simulation of propagation and coalescence of flaws in rock materials under compressive loads using the extended non-ordinary state-based peridynamics. *Engineering Fracture Mechanics*, *163*, 248–273.

[87] Gu, X., Madenci, E., & Zhang, Q. (2018). Revisit of non-ordinary state-based peridynamics. *Engineering fracture mechanics*, *190*, 31–52.

[88] Madenci, E., Dorduncu, M., Phan, N., & Gu, X. (2019). Weak form of bond-associated non-ordinary state-based peridynamics free of zero energy modes with uniform or non-uniform discretization. *Engineering Fracture Mechanics*, *218*, 106613.

[89] Hashim, N.A., Coombs, W., Augarde, C., & Hattori, G. (2020). An implicit non-ordinary state-based peridynamics with

stabilised correspondence material model for finite deformation analysis. *Computer Methods in Applied Mechanics and Engineering*, *371*, 113304.

[90] Ren, H., Zhuang, X., Cai, Y., & Rabczuk, T. (2016). Dual-horizon peridynamics. *International Journal for Numerical Methods in Engineering*, *108*(12), 1451–1476.

[91] Ren, H., Zhuang, X., & Rabczuk, T. (2017). Dual-horizon peridynamics: A stable solution to varying horizons. *Computer Methods in Applied Mechanics and Engineering*, *318*, 762–782.

[92] Rabczuk, T. & Ren, H. (2017). A peridynamics formulation for quasi-static fracture and contact in rock. *Engineering Geology*, *225*, 42–48.

[93] Rabczuk, T. & Zhuang, X. (2021). Dual-horizon peridynamics (DH-PD). In *Peridynamic Modeling, Numerical Techniques, and Applications*, Elsevier, 35–56.

[94] Macek, R.W. & Silling, S.A. (2007). Peridynamics via finite element analysis. *Finite elements in analysis and design*, *43*(15), 1169–1178.

[95] Lubineau, G., Azdoud, Y., Han, F., Rey, C., & Askari, A. (2012). A morphing strategy to couple non-local to local continuum mechanics. *Journal of the Mechanics and Physics of Solids*, *60*(6), 1088–1102.

[96] Azdoud, Y., Han, F., & Lubineau, G. (2013). A morphing framework to couple non-local and local anisotropic continua. *International Journal of Solids and Structures*, *50*(9), 1332–1341.

[97] Azdoud, Y., Han, F., & Lubineau, G. (2014). The morphing method as a flexible tool for adaptive local/non-local simulation of static fracture. *Computational Mechanics*, *54*(3), 711–722.

[98] Yaghoobi, A. & Chorzepa, M.G. (2018). Formulation of symmetry boundary modeling in non-ordinary state-based peridynamics and coupling with finite element analysis. *Mathematics and Mechanics of Solids*, *23*(8), 1156–1176.

[99] Wang, L., Xu, J., & Wang, J. (2019). Elastodynamics of linearized isotropic state-based peridynamic media. *Journal of Elasticity*, *137*(2), 157–176.

[100] Bode, T., Weißenfels, C., & Wriggers, P. (2020). Peridynamic Petrov–Galerkin method: a generalization of the peridynamic theory of correspondence materials. *Computer Methods in Applied Mechanics and Engineering*, *358*, 112636.

[101] Zhang, Q., Li, S., Zhang, A.M., Peng, Y., & Yan, J. (2021). A peridynamic Reissner-Mindlin shell theory. *International Journal for Numerical Methods in Engineering*, *122*(1), 122–147.

[102] Chowdhury, S.R., Roy, P., Roy, D., & Reddy, J. (2016). A peridynamic theory for linear elastic shells. *International Journal of Solids and Structures*, *84*, 110–132.

[103] Naumenko, K. & Eremeyev, V.A. (2021). A non-linear direct peridynamics plate theory. *Composite Structures*, 114728.

[104] O'Grady, J. & Foster, J. (2014). Peridynamic plates and flat shells: A non-ordinary, state-based model. *International Journal of Solids and Structures*, *51*(25-26), 4572–4579.

[105] Dorduncu, M., Kaya, K., & Ergin, O.F. (2020). Peridynamic analysis of laminated composite plates based on first-order shear deformation theory. *International Journal of Applied Mechanics*, *12*(03), 2050031.

[106] Yang, Z., Oterkus, E., Nguyen, C.T., & Oterkus, S. (2019). Implementation of peridynamic beam and plate formulations in finite element framework. *Continuum Mechanics and Thermodynamics*, *31*(1), 301–315.

[107] Bode, T., Weißenfels, C., & Wriggers, P. (2020). Mixed peridynamic formulations for compressible and incompressible finite deformations. *Computational Mechanics*, *65*(5), 1365–1376.

[108] Roy, P., Pathrikar, A., Deepu, S., & Roy, D. (2017). Peridynamics damage model

through phase field theory. *International Journal of Mechanical Sciences*, *128*, 181–193.

[109] Roy, P., Deepu, S., Pathrikar, A., Roy, D., & Reddy, J. (2017). Phase field based peridynamics damage model for delamination of composite structures. *Composite Structures*, *180*, 972–993.

[110] Mehrmashhadi, J., Bahadori, M., & Bobaru, F. (2020). On validating peridynamic models and a phase-field model for dynamic brittle fracture in glass. *Engineering Fracture Mechanics*, *240*, 107355.

[111] Roy, P., Pathrikar, A., & Roy, D. (2021). Phase field–based peridynamics damage model: Applications to delamination of composite structures and inelastic response of ceramics. In *Peridynamic Modeling, Numerical Techniques, and Applications*, Elsevier, 327–354.

[112] Wildman, R.A. & Gazonas, G.A. (2014). A finite difference-augmented peridynamics method for reducing wave dispersion. *International Journal of Fracture*, *190*(1), 39–52.

[113] Gu, X., Zhang, Q., Huang, D., & Yv, Y. (2016). Wave dispersion analysis and simulation method for concrete SHPB test in peridynamics. *Engineering Fracture Mechanics*, *160*, 124–137.

[114] Butt, S.N., Timothy, J.J., & Meschke, G. (2017). Wave dispersion and propagation in state-based peridynamics. *Computational Mechanics*, *60*(5), 725–738.

[115] Bažant, Z.P., Luo, W., Chau, V.T., & Bessa, M.A. (2016). Wave dispersion and basic concepts of peridynamics compared to classical nonlocal damage models. *Journal of Applied Mechanics*, *83*(11).

[116] Mutnuri, V. & Gopalakrishnan, S. (2020). A re-examination of wave dispersion and on equivalent spatial gradient of the integral in bond-based peridynamics. *Journal of Peridynamics and Nonlocal Modeling*, *2*(3), 243–277.

[117] Chan, W. & Chen, H. (2021). Peridynamic bond-associated correspondence model: Wave dispersion property. *International Journal for Numerical Methods in Engineering*.

[118] Yaghoobi, A. & Chorzepa, M.G. (2017). Higher-order approximation to suppress the zero-energy mode in non-ordinary state-based peridynamics. *Computers & Structures*, *188*, 63–79.

[119] Chen, H. & Chan, W. (2020). Higher-order peridynamic material correspondence models for elasticity. *Journal of Elasticity*, *142*(1), 135–161.

[120] Yang, Z., Oterkus, E., & Oterkus, S. (2021). Peridynamic modelling of higher order functionally graded plates. *Mathematics and Mechanics of Solids*, 10812865211004671.

[121] Yang, Z., Oterkus, E., & Oterkus, S. (2021). Peridynamic higher-order beam formulation. *Journal of Peridynamics and Nonlocal Modeling*, *3*(1), 67–83.

[122] Yang, Z., Oterkus, E., & Oterkus, S. (2021). Peridynamic formulation for higher-order plate theory. *Journal of Peridynamics and Nonlocal Modeling*, *3*(3), 185–210.

[123] Madenci, E., Barut, A., & Futch, M. (2016). Peridynamic differential operator and its applications. *Computer Methods in Applied Mechanics and Engineering*, *304*, 408–451.

[124] Madenci, E., Dorduncu, M., Barut, A., & Futch, M. (2017). Numerical solution of linear and nonlinear partial differential equations using the peridynamic differential operator. *Numerical Methods for Partial Differential Equations*, *33*(5), 1726–1753.

[125] Bazazzadeh, S., Shojaei, A., Zaccariotto, M., & Galvanetto, U. (2018). Application of the peridynamic differential operator to the solution of sloshing problems in tanks. *Engineering Computations*.

[126] Madenci, E., Barut, A., & Dorduncu, M. (2019). *Peridynamic differential operator for numerical analysis*. Springer.

[127] Shojaei, A., Galvanetto, U., Rabczuk, T., Jenabi, A., & Zaccariotto, M. (2019). A generalized finite difference method based on the Peridynamic differential operator for the solution of problems in bounded and unbounded domains. *Computer Methods in Applied Mechanics and Engineering*, *343*, 100–126.

[128] Dorduncu, M. (2019). Stress analysis of laminated composite beams using refined zigzag theory and peridynamic differential operator. *Composite Structures*, *218*, 193–203.

[129] Gao, Y. & Oterkus, S. (2019). Non-local modeling for fluid flow coupled with heat transfer by using peridynamic differential operator. *Engineering Analysis with Boundary Elements*, *105*, 104–121.

[130] Dorduncu, M. (2020). Stress analysis of sandwich plates with functionally graded cores using peridynamic differential operator and refined zigzag theory. *Thin-Walled Structures*, *146*, 106468.

[131] Gao, Y. & Oterkus, S. (2019). Nonlocal numerical simulation of low Reynolds number laminar fluid motion by using peridynamic differential operator. *Ocean Engineering*, *179*, 135–158.

[132] Dorduncu, M. & Apalak, M.K. (2020). Elastic flexural analysis of adhesively bonded similar and dissimilar beams using refined zigzag theory and peridynamic differential operator. *International Journal of Adhesion and Adhesives*, *101*, 102631.

[133] Gao, Y. & Oterkus, S. (2020). Fluid-elastic structure interaction simulation by using ordinary state-based peridynamics and peridynamic differential operator. *Engineering Analysis with Boundary Elements*, *121*.

[134] Gao, Y. & Oterkus, S. (2020). Multi-phase fluid flow simulation by using peridynamic differential operator. *Ocean Engineering*, *216*, 108081.

[135] Haghighat, E., Bekar, A.C., Madenci, E., & Juanes, R. (2021). A nonlocal physics-informed deep learning framework using the peridynamic differential operator. *Computer Methods in Applied Mechanics and Engineering*, *385*, 114012.

[136] Kan, X., Yan, J., Li, S., & Zhang, A. (2021). On differences and comparisons of peridynamic differential operators and nonlocal differential operators. *Computational Mechanics*, 1–19.

[137] Nguyen, C.T., Oterkus, S., Oterkus, E., Amin, I., Ozdemir, M., El-Aassar, A.H., & Shawky, H. (2021). Modelling of Eulerian incompressible fluid flows by using peridynamic differential operator. *Ocean Engineering*, *239*, 109815.

[138] Li, Z., Huang, D., Xu, Y., & Yan, K. (2021). Nonlocal steady-state thermoelastic analysis of functionally graded materials by using peridynamic differential operator. *Applied Mathematical Modelling*, *93*, 294–313.

[139] Bekar, A.C., Madenci, E., Haghighat, E., Waheed, U.b., & Alkhalifah, T. (2021). Solving the Eikonal equation for compressional and shear waves in anisotropic media using peridynamic differential operator. *arXiv preprint arXiv:210701268*.

[140] Rabczuk, T., Ren, H., & Zhuang, X. (2019). A nonlocal operator method for partial differential equations with application to electromagnetic waveguide problem. *Computers, Materials & Continua 59 (2019), Nr 1*.

[141] Ren, H., Zhuang, X., & Rabczuk, T. (2020). A nonlocal operator method for solving partial differential equations. *Computer Methods in Applied Mechanics and Engineering*, *358*, 112621.

[142] Ren, H., Zhuang, X., & Rabczuk, T. (2020). A higher order nonlocal operator method for solving partial differential

equations. *Computer Methods in Applied Mechanics and Engineering*, *367*, 113132.

[143] Ren, H., Zhuang, X., & Rabczuk, T. (2020). Nonlocal operator method with numerical integration for gradient solid. *Computers & Structures*, *233*, 106235.

[144] Ren, H., Zhuang, X., Trung, N.T., & Rabczuk, T. (2021). Nonlocal operator method for the Cahn-Hilliard phase field model. *Communications in Nonlinear Science and Numerical Simulation*, *96*, 105687.

[145] Ren, H., Zhuang, X., Trung, N.T., & Rabczuk, T. (2021). A nonlocal operator method for finite deformation higher-order gradient elasticity. *Computer Methods in Applied Mechanics and Engineering*, *384*, 113963.

[146] Ren, H., Zhuang, X., Anitescu, C., & Rabczuk, T. (2021). Multi-connected boundary conditions in solid mechanics and surgery theory. *Computers & Structures*, *251*, 106504.

[147] Zhang, Y., Ren, H., Areias, P., Zhuang, X., & Rabczuk, T. (2021). Quasi-static and dynamic fracture modeling by the nonlocal operator method. *Engineering Analysis with Boundary Elements*, *133*, 120–137.

[148] Zhuang, X., Ren, H., & Rabczuk, T. (2021). Nonlocal operator method for dynamic brittle fracture based on an explicit phase field model. *European Journal of Mechanics-A/Solids*, *90*, 104380.

[149] Zhang, Y. & Ren, H. (2022). Implicit implementation of the nonlocal operator method: an open source code. *Engineering with Computers*, 1–35.

[150] Zhang, Y. (2022). Nonlocal dynamic Kirchhoff plate formulation based on nonlocal operator method. *Engineering with Computers*, 1–15.

[151] Pian, T.H. & Chen, D. (1983). On the suppression of zero energy deformation modes. *International Journal for Numerical Methods in Engineering*, *19*(12), 1741–1752.

[152] Vignjevic, R., Campbell, J., & Libersky, L. (2000). A treatment of zero-energy modes in the smoothed particle hydrodynamics method. *Computer methods in Applied mechanics and Engineering*, *184*(1), 67–85.

[153] Breitenfeld, M., Geubelle, P., Weckner, O., & Silling, S. (2014). Non-ordinary state-based peridynamic analysis of stationary crack problems. *Computer Methods in Applied Mechanics and Engineering*, *272*, 233–250.

[154] Yee, K. (1966). Numerical solution of initial boundary value problems involving Maxwell's equations in isotropic media. *IEEE Transactions on antennas and propagation*, *14*(3), 302–307.

[155] Ward, A. & Pendry, J.B. (1996). Refraction and geometry in Maxwell's equations. *Journal of modern optics*, *43*(4), 773–793.

[156] Johnson, S.G. & Joannopoulos, J.D. (2001). Block-iterative frequency-domain methods for Maxwell's equations in a planewave basis. *Optics express*, *8*(3), 173–190.

[157] Fleisch, D. (2008). *A student's guide to Maxwell's equations*. Cambridge University Press.

[158] Huray, P.G. (2011). *Maxwell's equations*. John Wiley & Sons.

[159] Jin, J.M. (2015). *The finite element method in electromagnetics*. John Wiley & Sons.

[160] Gibson, W.C. (2007). *The method of moments in electromagnetics*. Chapman and Hall/CRC.

[161] Taflove, A. & Hagness, S.C. (2005). *Computational electrodynamics: the finite-difference time-domain method*. Artech house.

[162] Deschamps, G.A. (1972). Ray techniques in electromagnetics. *Proceedings of the IEEE*, *60*(9), 1022–1035.

[163] Ho, S., Yang, S., Machado, J.M., & Wong, H.c.C. (2001). Application of a meshless method in electromagnetics. *IEEE transactions on magnetics*, *37*(5), 3198–3202.

[164] Zhuang, X., Augarde, C., & Mathisen., K. (2012). Fracture modelling using meshless methods and level sets in 3D: framework and modelling. *International Journal for Numerical Methods in Engineering*, *92*, 969–998.

[165] Bouche, D., Molinet, F., & Mittra, R. (2012). *Asymptotic methods in electromagnetics*. Springer Science & Business Media.

[166] Chew, W.C., Jin, J.M., Lu, C.C., Michielssen, E., & Song, J.M. (1997). Fast solution methods in electromagnetics. *IEEE Transactions on Antennas and Propagation*, *45*(3), 533–543.

[167] Ehrlich, L.W. & Gupta, M.M. (1975). Some difference schemes for the biharmonic equation. *SIAM Journal on Numerical Analysis*, *12*(5), 773–790.

[168] Karageorghis, A. & Fairweather, G. (1987). The method of fundamental solutions for the numerical solution of the biharmonic equation. *Journal of Computational Physics*, *69*(2), 434–459.

[169] Abdulhadi, Z., Muhanna, Y.A., & Khuri, S. (2005). On univalent solutions of the biharmonic equation. *Journal of Inequalities and Applications*, *2005*(5), 1–10.

[170] Abdulhadi, Z., Muhanna, Y.A., & Khuri, S. (2006). On some properties of solutions of the biharmonic equation. *Applied Mathematics and Computation*, *177*(1), 346–351.

[171] Yang, B., Ding, H.j., & Chen, W.q. (2008). Elasticity solutions for functionally graded plates in cylindrical bending. *Applied Mathematics and Mechanics*, *29*(8), 999–1004.

[172] Wang, C., Wang, X., Zhang, X., & Hu, P. (2017). Assumed stress quasi-conforming technique for static and free vibration analysis of Reissner–Mindlin plates. *International Journal for Numerical Methods in Engineering*, *112*(4), 303–337.

[173] Finiukova, V.O. & Stolyar, A.M. (2011). Asymptotic Integration of One Narrow Plate Problem. In *Shell-like Structures*, Springer, 53–62.

[174] Librescu, L. & Lin, W. (1997). Postbuckling and vibration of shear deformable flat and curved panels on a non-linear elastic foundation. *International journal of non-linear mechanics*, *32*(2), 211–225.

[175] Galileev, S., Matrosov, A., & Verizhenko, V. (1995). Method of initial functions for layered and continuously inhomogeneous plates and shells. *Mechanics of Composite Materials*, *30*(4), 386–392.

[176] Faddeev, L. (1967). SCHRÖDINGER EQUATION. *Nine Papers on Partial Differential Equations and Functional Analysis*, *65*, 139.

[177] Tsutsumi, Y. (1987). Schrodinger equation. *Funkcialaj Ekvacioj*, *30*, 115–125.

[178] Laskin, N. (2002). Fractional schrödinger equation. *Physical Review E*, *66*(5), 056108.

[179] Berezin, F.A. & Shubin, M. (2012). *The Schrödinger Equation*, volume 66. Springer Science & Business Media.

[180] Fibich, G. (2015). *The nonlinear Schrödinger equation*. Springer.

[181] Poisson, S.D. (1826). *Mémoire sur la théorie du magnétisme en movement*. L'Académie.

[182] Weinert, M. (1981). Solution of Poisson's equation: Beyond Ewald-type methods. *Journal of Mathematical Physics*, *22*(11), 2433–2439.

[183] Dörfler, W. (1996). A convergent adaptive algorithm for Poisson's equation. *SIAM Journal on Numerical Analysis*, *33*(3), 1106–1124.

[184] Jackson, J.A. (2005). *Glossary of geology*.

[185] Föppl, A. (1897). *Vorlesungen über technische Mechanik*, volume 3. BG Teubner.

[186] Theodore, V. (1910). Festigkeits problem in maschinenbau, Encycl. *Der math Wiss*, *4*, 348–351.

[187] Cerda, E. & Mahadevan, L. (2003). Geometry and physics of wrinkling. *Physical review letters*, *90*(7), 074302.

[188] Landau, L. & Lifshitz, E. (1976), Theory of Elasticity. Theoretical Physics.

[189] Hibbett, Karlsson, & Sorensen (1998). *ABAQUS / standard: User's Manual*, volume 1. Hibbitt, Karlsson & Sorensen.

[190] Elliott, C.M. & French, D.A. (1987). Numerical studies of the Cahn-Hilliard equation for phase separation. *IMA Journal of Applied Mathematics*, *38*(2), 97–128.

[191] Bai, F., Elliott, C., Gardiner, A., Spence, A., & Stuart, A. (1995). The viscous Cahn-Hilliard equation. I. computations. *Nonlinearity*, *8*(2), 131.

[192] Da Prato, G. & Debussche, A. (1996). Stochastic cahn-hilliard equation. *Nonlinear Analysis: Theory, Methods & Applications*, *26*(2), 241–263.

[193] Elliott, C.M. & Stuart, A.M. (1996). Viscous Cahn–Hilliard equation II. Analysis. *journal of differential equations*, *128*(2), 387–414.

[194] Novick-Cohen, A. (2008). The cahn–hilliard equation. *Handbook of differential equations: evolutionary equations*, *4*, 201–228.

[195] Kim, B., Lee, S.B., Lee, J., Cho, S., Park, H., Yeom, S., & Park, S.H. (2012). A comparison among Neo-Hookean model, Mooney-Rivlin model, and Ogden model for chloroprene rubber. *International Journal of Precision Engineering and Manufacturing*, *13*(5), 759–764.

[196] Reese, S., Wriggers, P., & Reddy, B. (2000). A new locking-free brick element technique for large deformation problems in elasticity. *Computers & Structures*, *75*(3), 291–304.

[197] Korelc, J. & Wriggers, P. (2016). *Automation of Finite Element Methods*. Springer.

[198] Cosserat, E. (1909). François Cosserat. *Théorie des corps déformables*.

[199] Toupin, R. (1962). Elastic materials with couple-stresses. *Archive for rational mechanics and analysis*, *11*(1), 385–414.

[200] Toupin, R.A. (1964). Theories of elasticity with couple-stress.

[201] Hadjesfandiari, A. & Dargush, G. (2012). Boundary element formulation for plane problems in couple stress elasticity. *International Journal for Numerical Methods in Engineering*, *89*(5), 618–636.

[202] Mindlin, R.D. & Eshel, N. (1968). On first strain-gradient theories in linear elasticity. *International Journal of Solids and Structures*, *4*(1), 109–124.

[203] Mindlin, R.D. (1963). Microstructure in linear elasticity. Technical report, Columbia Univ New York Dept of Civil Engineering and Engineering Mechanics.

[204] Eringen, A.C. (1983). On differential equations of nonlocal elasticity and solutions of screw dislocation and surface waves. *Journal of applied physics*, *54*(9), 4703–4710.

[205] Polizzotto, C. (2012). A gradient elasticity theory for second-grade materials and higher order inertia. *International Journal of Solids and Structures*, *49*(15-16), 2121–2137.

[206] Papargyri-Beskou, S. & Beskos, D. (2010). Static analysis of gradient elastic bars, beams, plates and shells. *The Open Mechanics Journal*, *4*(1).

[207] Aravas, N. (2011). Plane-strain problems for a class of gradient elasticity models a stress function approach. *Journal of Elasticity*, *104*(1-2), 45–70.

[208] Charalambopoulos, A. & Polyzos, D. (2015). Plane strain gradient elastic rectangle in tension. *Archive of Applied Mechanics*, *85*(9), 1421–1438.

[209] Videla, J. & Atroshchenko, E. (2017). Analytical study of a circular inhomogeneity with homogeneously imperfect interface in plane micropolar elasticity. *ZAMM-Journal of Applied Mathematics and Mechanics/Zeitschrift für Angewandte Mathematik und Mechanik*, *97*(3), 322–339.

[210] Khakalo, S. & Niiranen, J. (2017). Gradient-elastic stress analysis near cylindrical holes in a plane under bi-axial tension fields. *International Journal of Solids and Structures*, *110*, 351–366.

[211] Shu, J.Y., King, W.E., & Fleck, N.A. (1999). Finite elements for materials with strain gradient effects. *International Journal for Numerical Methods in Engineering*, *44*(3), 373–391.

[212] Amanatidou, E. & Aravas, N. (2002). Mixed finite element formulations of strain-gradient elasticity problems. *Computer Methods in Applied Mechanics and Engineering*, *191*(15-16), 1723–1751.

[213] Askes, H. & Gutiérrez, M.A. (2006). Implicit gradient elasticity. *International Journal for Numerical Methods in Engineering*, *67*(3), 400–416.

[214] Darrall, B.T., Dargush, G.F., & Hadjesfandiari, A.R. (2014). Finite element Lagrange multiplier formulation for size-dependent skew-symmetric couple-stress planar elasticity. *Acta Mechanica*, *225*(1), 195–212.

[215] Atroshchenko, E. & Bordas, S.P. (2015). Fundamental solutions and dual boundary element methods for fracture in plane Cosserat elasticity. *Proceedings of the Royal Society A: Mathematical, Physical and Engineering Sciences*, *471*(2179), 20150216.

[216] Askes, H. & Aifantis, E.C. (2002). Numerical modeling of size effects with gradient elasticity-formulation, meshless discretization and examples. *International Journal of Fracture*, *117*(4), 347–358.

[217] Tang, Z., Shen, S., & Atluri, S. (2003). Analysis of materials with strain-gradient effects: A meshless local Petrov-Galerkin (MLPG) approach, with nodal displacements only. *Computer Modeling in Engineering and Sciences*, *4*(1), 177–196.

[218] Balobanov, V., Khakalo, S., & Niiranen, J. (2016). Isogeometric analysis of gradient-elastic 1D and 2D problems. In *Generalized Continua as Models for Classical and Advanced Materials*, Springer, 37–45.

[219] Khakalo, S. & Niiranen, J. (2017). Isogeometric analysis of higher-order gradient elasticity by user elements of a commercial finite element software. *Computer-Aided Design*, *82*, 154–169.

[220] Niiranen, J., Kiendl, J., Niemi, A.H., & Reali, A. (2017). Isogeometric analysis for sixth-order boundary value problems of gradient-elastic Kirchhoff plates. *Computer Methods in Applied Mechanics and Engineering*, *316*, 328–348.

[221] Makvandi, R., Reiher, J.C., Bertram, A., & Juhre, D. (2018). Isogeometric analysis of first and second strain gradient elasticity. *Computational Mechanics*, *61*(3), 351–363.

[222] Niiranen, J., Balobanov, V., Kiendl, J., & Hosseini, S. (2019). Variational formulations, model comparisons and numerical methods for Euler–Bernoulli micro-and nano-beam models. *Mathematics and Mechanics of Solids*, *24*(1), 312–335.

[223] Thanh, C.L., Ferreira, A., & Wahab, M.A. (2019). A refined size-dependent couple stress theory for laminated composite micro-plates using isogeometric analysis. *Thin-Walled Structures*, *145*, 106427.

[224] Reiher, J.C., Giorgio, I., & Bertram, A. (2017). Finite-element analysis of polyhedra under point and line forces in second-strain gradient elasticity. *Journal of Engineering Mechanics*, *143*(2), 04016112.

[225] Miehe, C., Hofacker, M., & Welschinger, F. (2010). A phase field model for rate-independent crack propagation: Robust algorithmic implementation based on operator splits. *Computer Methods in Applied Mechanics and Engineering*, *199*(45-48), 2765–2778.

[226] Miehe, C., Welschinger, F., & Hofacker, M. (2010). Thermodynamically consistent phase-field models of fracture: Variational principles and multi-field FE implementations. *International Journal for Numerical Methods in Engineering*, *83*(10), 1273–1311.

[227] Borden, M., Verhoosel, C., Scott, M., Hughes, T., & Landis, C. (2012). A phase-field description of dynamic brittle fracture. *Computer Methods in Applied Mechanics and Engineering*, *217*, 77–95.

[228] Hesch, C. & Weinberg, K. (2014). Thermodynamically consistent algorithms for a finite-deformation phase-field approach to fracture. *International Journal for Numerical Methods in Engineering*, *99*(12), 906–924.

[229] Rabczuk, T. (2013). Computational methods for fracture in brittle and quasi-brittle solids: state-of-the-art review and future perspectives. *International Scholarly Research Notices*, *2013*.

[230] Bourdin, B., Francfort, G.A., & Marigo, J.J. (2008). The variational approach to fracture. *Journal of elasticity*, *91*(1-3), 5–148.

[231] Feng, X., He, Y., & Liu, C. (2007). Analysis of finite element approximations of a phase field model for two-phase fluids. *Mathematics of computation*, *76*(258), 539–571.

[232] Tonks, M.R., Gaston, D., Millett, P.C., Andrs, D., & Talbot, P. (2012). An object-oriented finite element framework for multiphysics phase field simulations. *Computational Materials Science*, *51*(1), 20–29.

[233] Hesch, C., Schuß, S., Dittmann, M., Franke, M., & Weinberg, K. (2016). Isogeometric analysis and hierarchical refinement for higher-order phase-field models. *Computer Methods in Applied Mechanics and Engineering*, *303*, 185–207.

[234] Borden, M.J., Hughes, T.J., Landis, C.M., & Verhoosel, C.V. (2014). A higher-order phase-field model for brittle fracture: Formulation and analysis within the isogeometric analysis framework. *Computer Methods in Applied Mechanics and Engineering*, *273*, 100–118.

About Authors

Yongzheng ZHANG is currently a PhD candidate at the Institute of Structural Mechanics, Bauhaus-University Weimar, Germany. He received his Bachelor degree in Hydraulic and Hydro-Power Engineering in 2014, and Master degree in Geotechnical Engineering in 2017. His research interests are focused on nonlocal operator method, partial differential equations, peridynamics, finite element method and meshless methods.

Huilong REN is currently a research assistant in the department of Mathematics and Physics, Leibniz Hannover University of Hannover City, Germany. He received his B.S degree in Civil Engineering from the Chongqing University of China in 2011, and M.S degree in Civil Engineering from Tongji University of Shanghai City, China in 2014. He received a Ph.D. degree in Civil Engineering from Bauhaus University, Weimar of Germany in 2021. His research interest includes nonlocal operator methods, numerical methods and automatic programming.

Timon RABCZUK is currently professor at the Bauhaus University Weimar. He has received his PhD at University of Karlsruhe in 2002.